BJR http://dx.doi.org/10.1259/bjr.20150995

Received: 25 November 2015 | Revised: 11 January 2016 | Accepted: 3 March 2016

Cite this article as:
Reiter U, Reiter G, Fuchsjäger M. MR phase-contrast imaging in pulmonary hypertension. *Br J Radiol* 2016; **89**: 20150995.

REVIEW ARTICLE

MR phase-contrast imaging in pulmonary hypertension

[1]URSULA REITER, PhD, [2]GERT REITER, PhD and [1]MICHAEL FUCHSJÄGER, MD

[1]Division of General Radiology, Department of Radiology, Medical University of Graz, Austria
[2]Research and Development, Siemens Healthcare, Graz, Austria

Address correspondence to: Ursula Reiter
E-mail: *ursula.reiter@medunigraz.at*

Ursula Reiter and Gert Reiter contributed equal to this work.

ABSTRACT

Pulmonary hypertension (PH) is a life-threatening, multifactorial pathophysiological haemodynamic condition, diagnosed when the mean pulmonary arterial pressure equals or exceeds 25 mmHg at rest during right heart catheterization. Cardiac MRI, in general, and MR phase-contrast (PC) imaging, in particular, have emerged as potential techniques for the standardized assessment of cardiovascular function, morphology and haemodynamics in PH. Allowing the quantification and characterization of macroscopic cardiovascular blood flow, MR PC imaging offers non-invasive evaluation of haemodynamic alterations associated with PH. Techniques used to study the PH include both the routine two-dimensional (2D) approach measuring predominant velocities through an acquisition plane and the rapidly evolving four-dimensional (4D) PC imaging, which enables the assessment of the complete time-resolved, three-directional blood-flow velocity field in a volume. Numerous parameters such as pulmonary arterial mean velocity, vessel distensibility, flow acceleration time and volume and tricuspid regurgitation peak velocity, as well as the duration and onset of vortical blood flow in the main pulmonary artery, have been explored to either diagnose PH or find non-invasive correlates to right heart catheter parameters. Furthermore, PC imaging-based analysis of pulmonary arterial pulse-wave velocities, wall shear stress and kinetic energy losses grants novel insights into cardiopulmonary remodelling in PH. This review aimed to outline the current applications of 2D and 4D PC imaging in PH and show why this technique has the potential to contribute significantly to early diagnosis and characterization of PH.

INTRODUCTION

Pulmonary hypertension (PH), a life-threatening, multifactorial pathophysiological condition of the pulmonary circulation system, is diagnosed when the mean pulmonary arterial pressure (mPAP) equals or exceeds 25 mmHg at rest during right heart catheterization (RHC).[1,2] RHC is the clinical reference standard for the diagnosis of PH, as it allows haemodynamic characterization of the pulmonary circulation from the assessment of the right atrial pressure (RAP), pulmonary arterial pressure [diastolic pulmonary arterial pressure (dPAP); systolic pulmonary arterial pressure (sPAP); and mean pulmonary arterial pressure (mPAP)], pulmonary arterial wedge pressure (PAWP), cardiac output (CO), transpulmonary pressure gradient (TPG = mPAP−PAWP) and pulmonary vascular resistance (PVR = TPG/CO) (Figure 1). Based on the combination of the RHC parameters, underlying aetiology, clinical presentation and response to treatment, five groups of conditions that cause PH have been identified.[2,3]

Irrespective of the underlying cause, PH is associated with increased morbidity and mortality, especially if the diagnosis is established late in the course of disease;[4] therefore, non-invasive tests which enable the identification of PH during routine clinical examinations are of great relevance for PH patient management.[4–6] Echocardiography is currently the most widely used modality for the non-invasive evaluation of patients with suspected PH.[1,7] Cardiac MRI in general and MR phase-contrast (PC) imaging in particular, however, have emerged as potential techniques for the standardized assessment of cardiac and myocardial function, morphology and myocardial viability.[8,9] Cardiac MR is useful for identifying alterations in the myocardial structure and morphology, and abnormalities in various parameters have been reported in PH,[6,10–14] including increased ventricular mass index, right ventricular hypertrophy and enlargement of the right ventricular cavity,[15] paradoxical movement of the intraventricular septum[16–18] and late gadolinium enhancement at the ventricular insertion points,[18–21] as well as dilatation and stiffening of the pulmonary artery vasculature.[22–24]

In addition to the morphological evaluation of the myocardium and the assessment of right and left ventricular

Figure 1. Schematic drawing indicating haemodynamic parameters typically assessed by right heart catheterization (RHC) and clinical PH groups. Arrows sketch the localization of the origin of disease. CO, cardiac output; CTEPH, chronic thromboembolic pulmonary hypertension; LA, left atrium; mPA, main pulmonary artery; PAH, pulmonary arterial hypertension; PAP, pulmonary arterial pressure; PAWP, pulmonary arterial wedge pressure; PH-LHD, pulmonary hypertension due to left heart disease; PH-lung, PH due to lung diseases; PV, pulmonary veins; PVR, pulmonary vascular resistance; RA, right atrium; RAP, right atrial pressure; RV, right ventricle; TPG, transpulmonary pressure gradient.

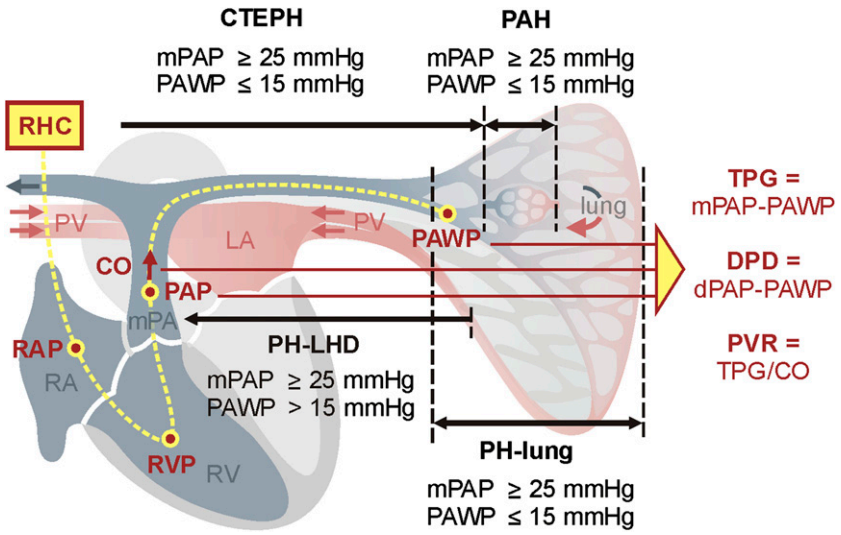

function indices by cardiac MRI techniques, MR PC imaging enables the assessment and investigation of blood velocities and blood flow fields in the cardiovascular system.[25–27] Generically related to pressure gradients therein, PC velocity mapping of the main pulmonary artery (mPA), pulmonary arterial tree, pulmonary veins, atrioventricular junctions and myocardial tissue provides metrics to not only estimate pulmonary pressures and PVR but also to characterize the pulmonary circulation more extensively than can be done with parameters derived from RHC alone. This review aimed to outline the applications of two-dimensional (2D, time-resolved one-directional velocity assessment) and four-dimensional (4D, time-resolved three-directional velocity assessment) PC imaging in PH and show that this technique has the potential to significantly contribute to early diagnosis and characterization of PH.

PHASE-CONTRAST IMAGING

MR PC imaging allows the measurement of the generically pulsatile and tridirectional macroscopic cardiovascular blood flow. Whereas the most commonly applied 2D PC imaging technique provides time-resolved velocity information in a typically predominant direction of motion, 4D PC imaging aims to assess the complete time-varying tridirectional velocity field in a volume of interest. A brief outline of the general aspects of the techniques will be given; a more comprehensive discussion can be found in, among other publications, those of Gatehouse et al[28] or Nayak et al[29] for 2D PC imaging and in Markl et al,[30,31] Hope et al[32] or Dyverfeldt et al[33] for 4D PC imaging.

Two-dimensional phase-contrast imaging

The MR signal of a voxel is a vector quantity possessing a magnitude and a direction (phase). Whereas usually only the magnitude of the signal is used for MR image reconstruction, PC imaging also exploits its phase to quantify the velocity of the tissue within the voxel. This is enabled by introducing an additional velocity-encoding gradient switching in the MR signal acquisition, which causes phase shifts proportional to blood and tissue velocities in the gradient direction. To extract these phase shifts proportional to the velocity, PC imaging acquires signals with and without switching of the velocity-encoding gradient and subtracts the resulting phases of voxels. The calculated phase shifts are transformed into a greyscale PC velocity image, where no phase shift—or equivalently no velocity—is represented by mid-grey, and phase shifts or velocities in either of the opposite directions are displayed correspondingly brighter or darker. Moreover, as the data of the reference measurement without velocity-encoding gradient switching can be employed to reconstruct a magnitude image, PC imaging typically provides assessment of anatomic and velocity images at once.

Owing to the pulsatile nature of cardiovascular blood flow, it is adequate to fuse the concept of PC imaging with that of physiological triggering (electrocardiographical or pulse gating) and cine imaging techniques. The principle of the resulting 2D PC MR sequence is illustrated in Figure 2. The underlying MR signal acquisition is typically realized as a 2D velocity-compensated, spoiled gradient-echo sequence. Techniques from conventional cine MRI like segmentation (acquisition of several data lines per data set in the cardiac cycle) or prospective and retrospective gating directly transpose to 2D PC sequences. Although 2D PC sequences double up the imaging time compared with conventional magnitude imaging, segmentation allows acquisition with a time resolution below 50 ms and a spatial in-plane resolution in the order of $1.5 \times 2.5\ mm^2$ during one breath-hold period. Retrospective gating facilitates complete coverage of the cardiac cycle and optionally the rejection of arrhythmic heart beats.

Figure 2. Principle of an electrocardiographically (ECG)-gated two-dimensional phase-contrast sequence. Segmentation is usually performed by interleaved acquisition of more (here three) data lines with and without velocity encoding per heartbeat. The principle of reconstruction of velocity (red) and magnitude (blue) images is indicated for three pixels (P) in one frame.

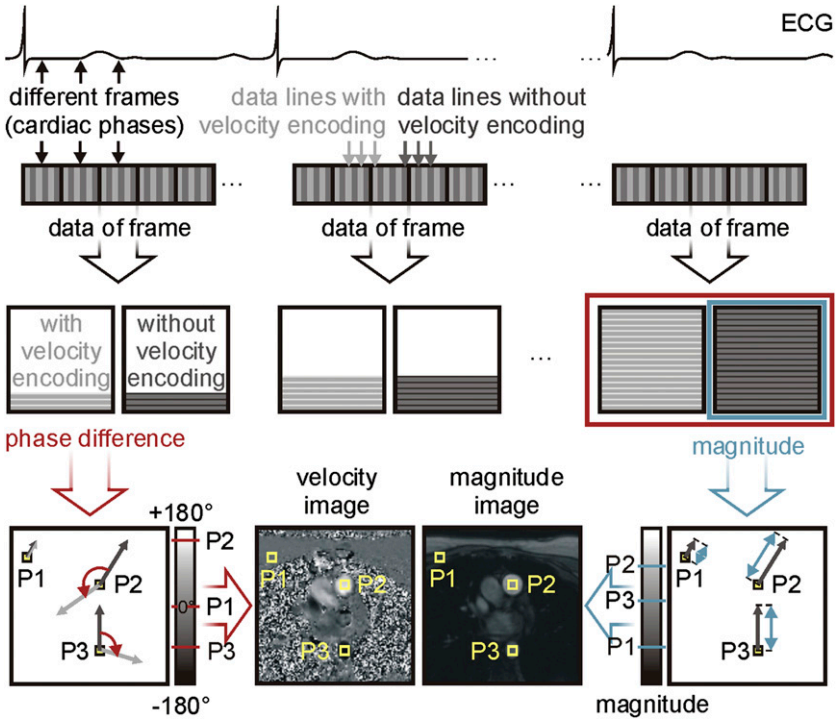

The proportionality constant between the velocity and the corresponding phase shift or grey value, which is ultimately determined by the form of velocity-encoding gradient switching, is adjusted by pre-defining the so-called velocity-encoding value (VENC); by definition, VENC represents the velocity causing phase shifts of 180°. VENC is usually chosen to be as small as possible while omitting velocity aliasing in the region of interest (Figure 3): whereas a smaller VENC increases the signal-to-noise ratio of PC velocity images, the absence of velocity aliasing prevents reinterpretation of erroneously represented velocities. Because peak velocities are unknown prior to measurement, VENC has to be optimized either iteratively or based on fast 2D PC "scout" measurements.

Figure 3. Impact of the choice of velocity-encoding value (VENC). Three two-dimensional phase-contrast measurements through the main pulmonary artery were performed consecutively in a healthy volunteer; the same systolic phase is shown. VENC = 300 cm s^{-1} (left panel): maximum velocities are much smaller than VENC and cause consequently only small phase differences, low contrast to stationary tissue and bad signal-to-noise ratio. VENC = 90 cm s^{-1} (mid panel): maximum velocities are close to VENC and cause phase differences close to 180°, high contrast to stationary tissue and good signal-to-noise ratio. VENC = 60 cm s^{-1} (right panel): maximum velocities are higher than VENC and cause phase differences larger 180°, which are erroneously represented as velocities in the opposite direction. This phenomenon is called aliasing.

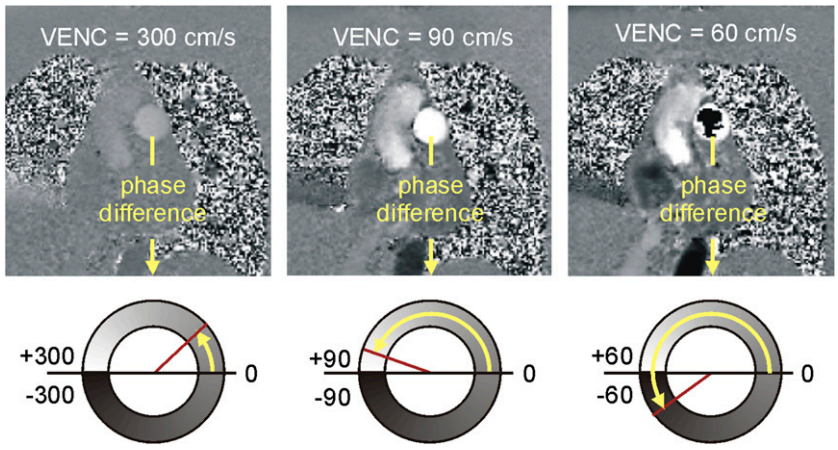

2D PC sequences are typically applied to characterize velocity in a predominant flow direction, such as that of blood flow along a vessel or through a cardiac valve; the imaging plane is usually chosen perpendicular to the predominant flow direction, and the through-plane velocity is assessed by switching velocity-encoding gradients in the slice-encoding direction. The latter approach provides cine images of velocities across the total cross-sectional area of the flow of interest, which allow first of all the determination of time courses of cross-sectional areas, maximal velocities (pixels with the highest velocities in the cross-sections), peak velocity (pixel with the highest velocity in the cardiac cycle) and time courses of mean velocities across that cross-sectional area. Moreover, time courses of flow (volume per time) through the cross-section can be calculated by multiplication of the cross-sectional area and mean through-plane velocity in every time frame. Integration of flow with respect to time finally results in the flow volume passing the cross-section in the cardiac cycle.

All these calculations are performed by suitable post-processing software after segmentation of cross-sections. Notably, cine PC velocity images may contain an artificial, spatially varying velocity offset, which, although small compared with VENC, might significantly distort determined flow volumes. From the viewpoint of acquisition, velocity offsets can be reduced by decreasing the distance between the flow of interest and the magnetic isocentre. In addition, velocity offsets can be estimated and corrected *a posteriori*, whereupon methodologies that aim to correct velocity offsets via spatial interpolation of velocities of stationary tissue appear more practical than the replicated 2D PC measurement in a resting phantom.

Four-dimensional phase-contrast imaging

Velocity is a vector quantity, and in order to specify this vector completely, its three spatial components have to be determined. As PC imaging measures velocity components in the velocity-encoding gradient direction, the simplest 4D PC technique is the successive acquisition of three 2D PC sequences with velocity encoding in phase encoding, read out and slice-selection directions, respectively. Velocity vectors can be reconstructed from the three orthogonal velocity components in any pixel of the imaging plane in any time frame (Figure 4); by sequential measurement of parallel imaging planes, a volume of interest can be covered.

Figure 4. Principle of three-directional phase-contrast imaging data acquisition. A velocity vector is specified by its two in-plane and one through-plane components.

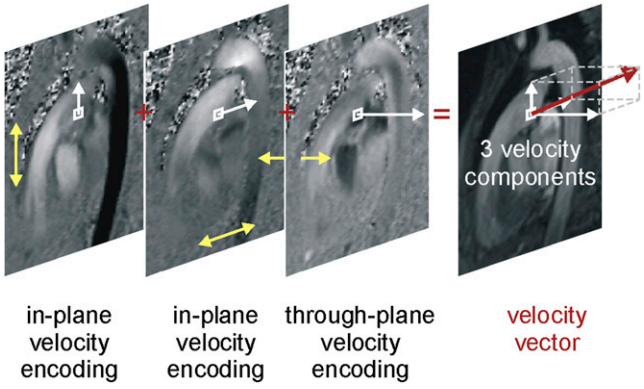

The speed of the above 4D PC image acquisition can be improved by measuring reference data without velocity-encoding gradients only once instead of three times. Typically, such a "4-point scheme" (four measurements for three velocity components) is implemented in a 4D PC sequence acquiring repeatedly velocity-compensated and all three velocity-encoded data lines. Furthermore, the application of spatial three-dimensional instead of two-dimensional 4D PC sequences facilitates spatial isotropic or close to isotropic resolutions.

Because tridirectional velocity encoding doubles up the imaging time of one-directional velocity encoding, 4D PC sequences are acquired even in the 2D case while the subject is breathing. Corresponding image ghosting and blurring can be alleviated by usage of respiratory motion-compensating techniques (averaging or respiratory gating) at further cost of imaging time. However, with suitable accelerated acquisition, 4D PC imaging times of around 10 minutes to cover large vessels or cardiac chambers with time resolution below 50 ms and spatial resolution in the order of $2.5 \times 2.5 \times 2.5\ mm^3$ can be achieved.

4D PC data contain complete flow information, in principle. Its extraction depends heavily on post-processing and suitable software. After application of some data pre-processing steps including corrections for possible aliasing or velocity offsets, the primary analysis tools are cross-sections and visualization of the acquired velocity field. By defining cross-sections on multiplanar reconstructed planes, 4D PC data allow the determination of maximal velocities, peak velocities, mean velocities, flow and flow volume through the cross-section similar to 2D PC imaging. In contrast to the 2D PC imaging technique, flow results can be derived and related at any cross-section within the covered volume *a posteriori*.

Vector plots as well as streamline and particle trace visualization represent the principal methods to visualize an acquired velocity field (Figure 5). Vector plots directly display measured velocity vectors as arrows in space; their length (often additionally colour encoded) corresponds to the velocity magnitude, their direction to the velocity direction. When densely scattered in a volume, the arrows obscure each other, such that vector plots are typically restricted to selectable cut-planes. Streamlines, defined as tangent curves to velocity vectors at a particular time point, describe instantaneous velocity directions in the volume; particle traces show the trajectories of particles moving in the velocity field, providing a time-integrated picture of flow. With adequate choice of starting (seeding) points, both types of curves provide a better volumetric impression of flow patterns than vector plots. Moreover, colour encoding enables the display of additional features like magnitude of velocity or curve origin.

STANDARD PC PARAMETERS OF THE MAIN PULMONARY ARTERY IN PH

Through-plane 2D PC imaging assessment of blood flow in the mPA is an integral part of various disease-oriented cardiac MR

Figure 5. Examples of a vector plot, streamline and a particle trace visualization of the same four-dimensional phase-contrast data set of a healthy volunteer displayed on maximum intensity projection for anatomic orientation. Vector plot showing three-dimensional velocity vectors projected on a multiplanar reconstructed cut-plane through the superior vena cava (SVC), inferior vena cava (IVC), right atrium (RA) and right ventricle (RV) in end-systole. Velocity magnitude is colour encoded (a). Streamline visualization demonstrating the three-dimensional tangent curves to the velocity vectors in end-systole. Seeding points were placed in the IVC, SVC and right ventricular outflow tract; velocity magnitude is colour encoded (b). Particle trace visualization showing the three-dimensional paths of particles in end-systole, which were seeded in the IVC (blue) and SVC (red) in end-diastole.

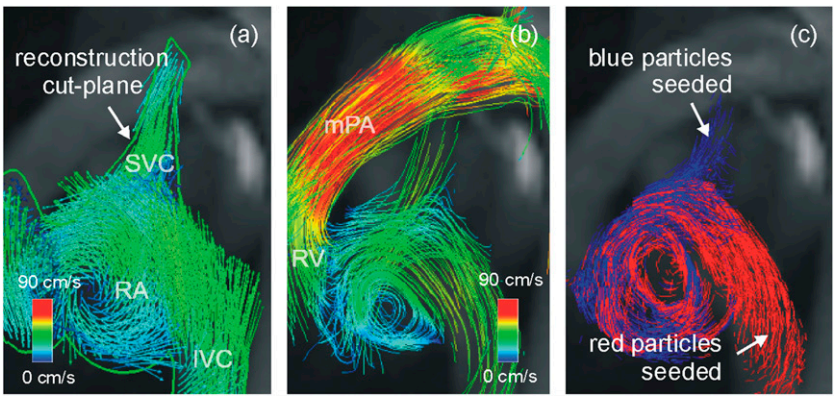

examinations, typically focusing on the determination of right ventricular stroke volume (RVSV) (passing flow volume in the cardiac cycle), regurgitation volume (diastolic backward flow volume) or shunt volume (difference to left ventricular stroke volume).[34,35] The imaging plane is positioned midway between the level of the pulmonary valve and the bifurcation of the branch pulmonary arteries and aligned so as to be perpendicular to the course of the vessel (Figure 6). To prescribe a plane

Figure 6. Planning of a through-plane two-dimensional phase-contrast imaging acquisition plane (a, b) in the main pulmonary artery (solid line) together with the resulting magnitude (c) and velocity (d) images. For evaluation of pulmonary arterial blood flow, the vessel cross-sectional area is usually segmented on the magnitude (solid contour) and transferred to the phase image (dotted contour).

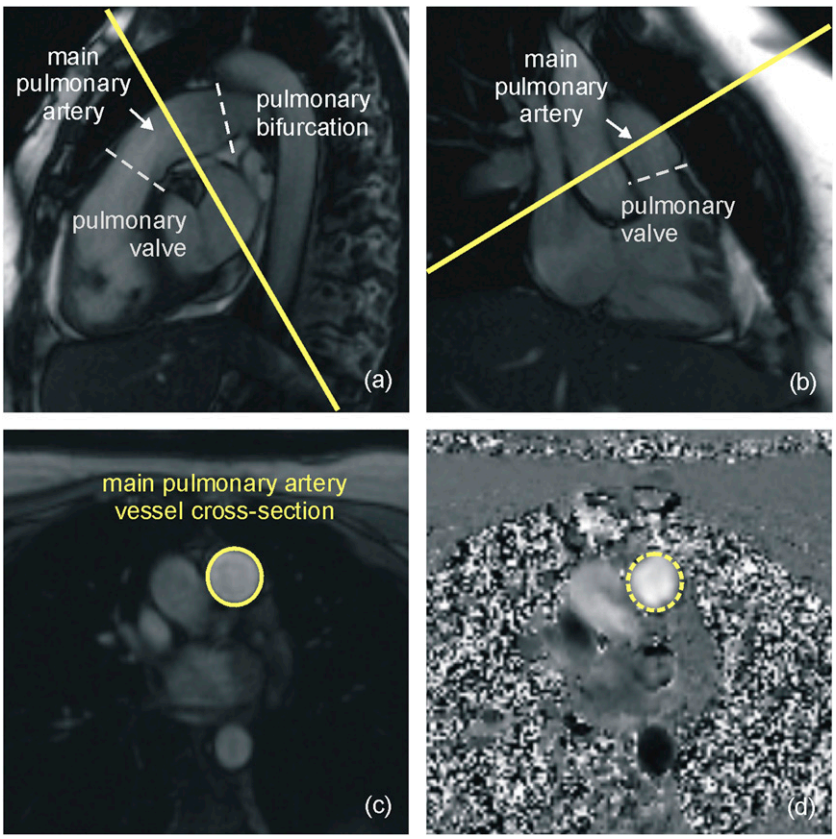

oriented truly perpendicularly to the mPA, and to ensure that the imaging plane remains between the pulmonary valve and the pulmonary artery bifurcation throughout the whole cardiac cycle, two double-oblique cine MR views oriented along the main axis of the pulmonary trunk are used for planning. As the pulmonary artery moves throughout the cardiac cycle, the cut-plane is defined in a systolic phase to ensure optimal image angulation in phases of the vast majority of blood flow. In general, this flow measurement in the pulmonary artery is considered to be precise,[35] especially when adequate velocity offset correction is applied.[36,37] Remarkably, breathing manoeuvres during acquisition (breathing, breath-hold in expiration or inspiration) significantly alter flow results.[38–40]

Alterations in a variety of parameters directly deducible from through-plane 2D PC measurement in the mPA have been documented in PH in both pre-clinical[41–43] and clinical studies, and the results have been related to RHC haemodynamic parameters and disease progression. The basic and most recent findings for these "standard" parameters are summarized.

Pulmonary artery vessel cross-section

In PH, pulmonary artery vessel distension progressively causes the reduction of the compliance of the pulmonary vascular bed, resulting in vessel wall stiffening.[22–24] Pulmonary artery stiffness, which is inversely proportional to vessel distensibility, is associated with right ventricular dysfunction[44,45] and mortality in patients with PH;[23,45–47] therefore, the assessment of pulmonary artery distensibility is an important parameter in the evaluation of PH.

The mPA distensibility can be derived from the relative cross-sectional area change (RAC) between systole (A_{max}) and diastole (A_{min}) *via* segmentation of the vessel area throughout the cardiac cycle (Figure 7a). Irrespective of the PH group, numerous studies have documented significantly increased A_{min} and decreased RAC in patients with PH (Table 1). Even though correlations of the mPA cross-sectional areas and RAC with mPAP or PVR are only moderate, A_{min} and RAC revealed high performance for PH diagnosis. Sanz et al[48] reported that $A_{min} \geq 6.6\,cm^2$ enabled diagnosis of PAH with sensitivity/specificity of 93%/88%, and $A_{min} \geq 6.0\,cm^2$ detected PVR >3 WU with sensitivity/specificity of 96%/85%. In line with these findings, Swift et al[15] showed that in a population including all PH groups, mPAP ≥ 25 mmHg can be identified from $A_{min} \geq 6.0\,cm^2$ with sensitivity/specificity of 88%/66%. Moreover, they identified decreased RAC as an early marker for increased PVR.[46]

Pulmonary arterial blood flow velocity

Decreased blood flow velocities (Figure 7b,c) in the mPA have been widely described in patients with PH (Table 2); a decrease of mean velocity in a vessel typically accompanies vessel dilatation. Whereas peak velocities correlate only moderately with mPAP or PVR, the average mean velocity ($v_{mean,avg}$) was found to be a potential parameter for diagnosing PH. Sanz et al[47] reported strong correlations of $v_{mean,avg}$ with mPAP ($r = -0.73$) and PVR ($r = -0.86$) in patients with PAH; a cut-off value of $11.7\,cm\,s^{-1}$ revealed a high accuracy to identify mPAP ≥ 25 mmHg (sensitivity/

Figure 7. Evaluation of a through-plane two-dimensional phase-contrast measurement in the main pulmonary artery. Time course of the vessel cross-sectional area (a): area change (AC) and relative area change (RAC) are calculated from minimum cross-sectional area (A_{min}) and maximum cross-sectional area (A_{max}); time course of the maximum velocity (b): peak velocity (v_{peak}) is indicated; time course of the mean velocity (c): time to peak (TTP) is defined as the time interval between onset of blood flow and maximum mean velocity ($v_{mean,max}$); the ejection time (ET) is time interval between onset and end ($v_{mean} = 0\,cm\,s^{-1}$) of systolic pulmonary arterial blood flow; time course of the pulmonary blood flow (d): acceleration time (AT) is defined as time interval between onset of blood flow and peak flow (Q_{peak}); maximum change in flow rate during ejection (dQ/dt_{max}) and acceleration volume (AccV) are indicated. The subscript avg denotes the average with respect to all cardiac phases. RR, cardiac interval.

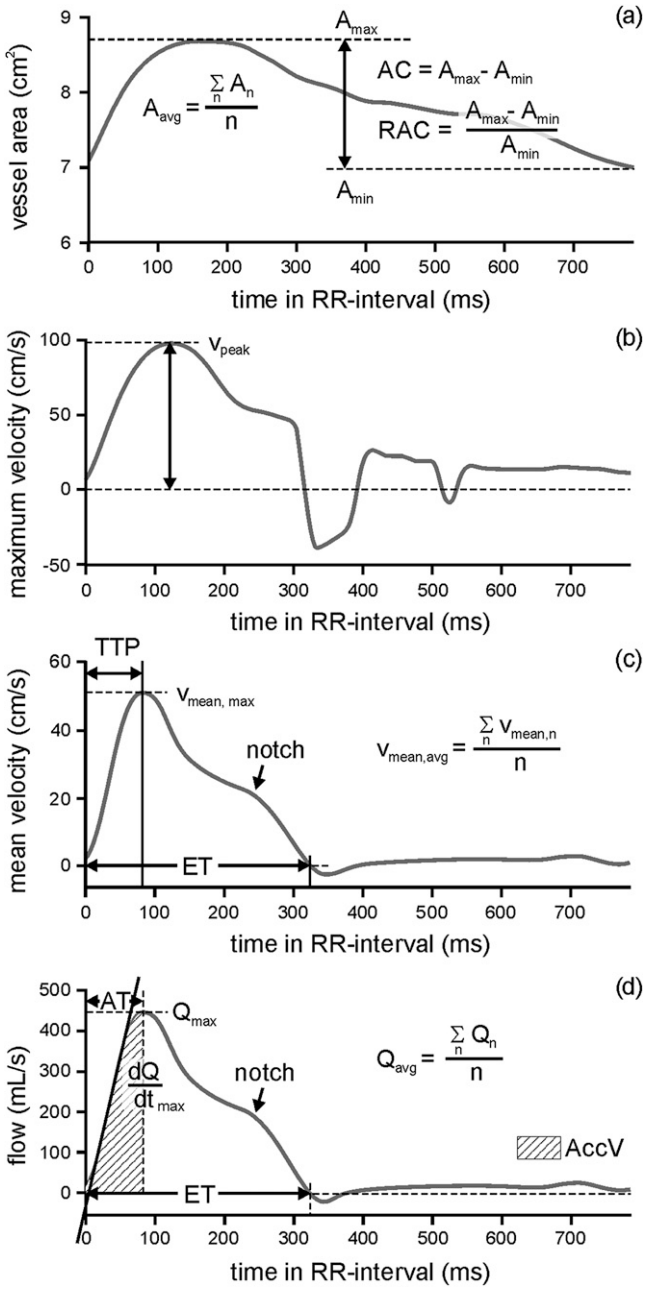

Table 1. Parameters derived from the time course of the main pulmonary artery vessel cross-sectional area obtained from MR phase-contrast measurements and their correlation to the mean pulmonary artery pressure (mPAP) and pulmonary vascular resistance (PVR)

Reference	PH	Non-PH	Correlation mPAP/PVR	Comment
A_{max} (cm^2)				
Sanz et al[48]	11.8 ± 3.7	7.1 ± 2.8	0.61/0.56	42 patients with PAH, 17 non-PH patients; linear correlation with mPAP and indexed PVR
Sanz et al[47]	10.7 (9.0–12.3)	7.1 (5.2–8.2)	0.51/0.43	75 patients with PH (all groups), 13 non-PH patients; linear correlation with mPAP and indexed PVR. Data given as median (interquartile range)
Jardim et al[22]	14.1 ± 6.0	–	–	19 patients with PAH
Swift et al[15]	9.7 ± 2.8	7.8 ± 4.6	0.28/0.17	106 patients with PH (all groups) and non-PH patients; non-significant linear correlation with PVR. $AUC_{mPAP>25mmHg} = 0.77$; cut-off = 8 cm^2; sensitivity/specificity = 74%/67%
Normalized A_{max}/BSA ($cm^2\,m^{-2}$)				
Moral et al[49]	6.1 ± 1.7	4.2 ± 1.0	0.42/–	152 patients with PH (all groups), 33 non-PH patients; linear correlation with mPAP
Garcia-Alvarez et al[50]	5.6 ± 2.0* 5.7 ± 3.0#	–	–/0.47*	*Derivation cohort: 80 patients with PH (all groups). #Validation cohort: 20 patients with PH (all groups)
A_{avg} (cm^2)				
Ley et al[27]	9 ± 2	6 ± 1	–	22 patients with PAH, 25 healthy controls
Sanz et al[48]	10.7 ± 3.5	6.1 ± 2.1	0.65/0.61	42 patients with PAH, 17 non-PH patients; linear correlation with mPAP and indexed PVR
A_{min} (cm^2)				
Sanz et al[48]	9.7 ± 3.6	4.8 ± 2.1	0.67/0.64	42 patients with PAH, 17 non-PH patients; linear correlation with mPAP and indexed PVR. $AUC_{mPAP>25mmHg} = 0.95$; cut-off = 6.6 cm^2; sensitivity/specificity = 93%/88%. $AUC_{PVR>3WU} = 0.93$; cut-off = 6.0 cm^2; sensitivity/specificity = 96%/85%
Helderman et al[51]	10.2 ± 2.2	4.9 ± 1.2	$R^2 = 0.57$/–	38 patients with PAH, 17 non-PH patients
Sanz et al[47]	8.5 (7.5–10.5)	4.5 (3.9–5.8)	0.58/0.50	75 patients with PH (all groups), 13 non-PH patients; linear correlation with mPAP and indexed PVR. Data given as median (interquartile range)
Swift et al[15]	8.9 ± 2.8	6.7 ± 4.7	0.35/0.26	106 patients with PH (all groups) and non-PH patients; linear correlation with mPAP and PVR. $AUC_{mPAP>25mmHg} = 0.82$; cut-off = 6 cm^2; sensitivity/specificity = 88%/66%
Jardim et al[22]	12.6 ± 6.0	–	–	19 patients with PAH
Normalized A_{min}/BSA ($cm^2\,m^{-2}$)				
Moral et al[49]	5.1 ± 1.5	3.0 ± 0.8	0.49/–	152 patients with PH (all groups), 33 non-PH patients; linear correlation with mPAP
Garcia-Alvarez et al[50]	4.6 ± 1.8* 4.2 ± 3.3#	–	–/0.54	*Derivation cohort: 80 patients with PH (all groups). #Validation cohort: 20 patients with PH (all groups)
RAC (%)				
Sanz et al[48]	17 ± 13	49 ± 33	−0.52/−0.57	42 patients with PAH, 17 non-PH patients; linear correlation with mPAP and indexed PVR

(Continued)

Table 1. (Continued)

Reference	PH	Non-PH	Correlation mPAP/PVR	Comment
Sanz et al[47]	17 (14–22)	55 (27–64)	−0.48/−0.47	75 patients with PH (all groups), 13 non-PH patients; linear correlation with mPAP and indexed PVR. AUC $_{mPAP>25mmHg}$ = 0.91; cut-off = 40%; sensitivity/specificity = 93%/63%. Data given as median (interquartile range)
Moral et al[49]	18 ± 10	40 ± 31	−0.45/–	152 patients with PH (all groups), 33 non-PH patients; linear correlation with mPAP
Swift et al[46]	8.8 ± 6.7* 4.9 ± 2.9#	18 ± 8	–/R^2 = 0.34	115 patients with PH (all groups; *97 survivors, #18 non-survivors), 19 non-PH patients. Inverse relation with PVR. $AUC_{mPAP>25mmHg}$ = 0.87; cut-off = 15%; sensitivity/specificity = 84%/74%
Swift et al[15]	8 ± 7	18 ± 7	−0.54/−0.54	106 patients with PH (all groups) and non-PH patients; linear correlation with mPAP and PVR. $AUC_{mPAP>25mmHg}$ = 0.87; cut-off = 15%; sensitivity/specificity = 86%/70%
Helderman et al[51]	6 ± 3	16 ± 10	–	38 patients with PAH, 17 non-PH patients
Truong et al[52]	21 ± 11	32 ± 18	–	25 paediatric patients with PAH, 4 paediatric healthy controls. Non-significant difference
Jardim et al[22]	14 ± 11	–	−0.25/−0.28	19 patients with PAH. Non-significant linear correlation with mPAP and PVR. AUC = 0.83; cut-off = 10% to differentiate acute vasodilator responders from non-responders: sensitivity/specificity = 100%/56%
Garcia-Alvarez et al[50]	19 ± 19* 22 ± 21#	–	–/−0.38	*Derivation cohort: 80 patients with PH (all groups). #Validation cohort: 20 patients with PH (all groups)
Kang et al[44]	19 ± 11	–	–/R^2 = 0.34	35 patients with PAH. Correlation with 6MWT: R^2 = 0.61. $AUC_{6MWT<400m}$ = 0.94; cut-off = 20%; sensitivity/specificity = 82%/94%
Rolf et al[53]	30 ± 19* 26 ± 12#	–	–	57 patients with CTEPH *pre- and #post endarterectomy

6MWT, 6-min walk test; A_{avg}, average cross-sectional area; A_{max}, maximal cross-sectional area; A_{min}, minimal cross-sectional area; AUC, area under the curve; BSA, body surface area; CTEPH, chronic thromboembolic pulmonary hypertension; PAH, pulmonary arterial hypertension; PH, pulmonary hypertension; RAC, relative cross-sectional area change.

specificity, 93%/82%) or PVR >3 WU (sensitivity/specificity, 91%/93%). Including all PH groups, Garcia-Alvarez et al[50] demonstrated a curvilinear (logarithmic) association of $v_{mean,avg}$ with PVR and showed that $v_{mean,avg}$ was the standard PC imaging parameter with the strongest univariate correlation with PVR, irrespective of the cause and severity of PH.

A prominent characteristic of the time course of v_{mean} in PH is an abnormal mid-systolic velocity deceleration (notch) (Figure 7c); this notch occurs later in systole in patients with PAH than in patients with proximal pulmonary embolism[58] and was introduced by Hardziyenka et al[59] as an easily assessable echocardiographic index for predicting the risk, in-hospital mortality and efficacy of pulmonary endarterectomy (PEA) in patients with chronic thromboembolic pulmonary hypertension (CTEPH). In a recent study, Rolf et al[53] showed that in patients with CTEPH, after PEA, the notch disappeared in the majority of patients in parallel with an increase of v_{peak}. Primarily attributable to increased wave reflection in the pulmonary artery,[53,58] the timing of the notch (early *vs* late) could be used to distinguish proximal *vs* distal obstructions in patients with acute pulmonary embolism.[60] Moreover, the presence of the notch 6 months after pulmonary embolism was related to poor right systolic function, reduced RAC and the development of CTEPH.

Pulmonary arterial blood flow, right ventricular stroke volume and cardiac output

Alterations in the mPA blood flow (Figure 7d) have already been analyzed in early studies employing 2D PC imaging in PH (Table 3). Authors reported shortened acceleration times (ATs) (time interval from the beginning of the anterograde flow in systole to peak systolic flow) and reduced passing blood volumes during that time (AccV, acceleration volume) in PH, reflecting increased PVR and the impairment of the right ventricular ejection function.[27,62,63] Mousseaux et al[62] documented a strong correlation between PVR and the quotient of maximum change in flow rate during ejection by AccV (r = 0.89). Moreover, Sugimoto et al[64] found that the maximum change in flow rate during ejection, when normalized to the body surface area, was

Table 2. Parameters derived from the time course of main pulmonary artery velocities obtained from MR phase-contrast measurements and their correlation to the main pulmonary arterial pressure (mPAP) and pulmonary vascular resistance (PVR)

Reference	PH	Non-PH	Correlation mPAP/PVR	Comment
v_{peak} (cm s^{-1})				
Ley et al[54]	32 ± 16* 50 ± 23#	82 ± 21	−0.6/−0.5	35 patients with CTEPH (*pre- and #post pulmonary thromboendarterectomy), 10 healthy controls
Ley et al[27]	72 ± 22	83 ± 11	−0.34/–	22 patients with PAH, 25 healthy controls. Non-significant correlation with mPAP
Sanz et al[48]	64 ± 26	84 ± 22	−0.37/−0.51	42 patients with PAH, 17 non-PH patients linear correlation with mPAP and indexed PVR
Guo et al[55]	53 ± 15	80 ± 17	−0.48/−0.41	20 patients with CTEPH, 20 healthy controls. Linear correlation with mPAP and indexed PVR
Helderman et al[51]	60 ± 21	88 ± 22	–	38 patients with PAH, 17 non-PH patients
Barker et al[56]	67 ± 22	84 ± 12	–	10 patients with PAH, 9 healthy controls (2 centres). Evaluation from 4D PC imaging
Truong et al[52]	80 ± 50	130 ± 70	–	25 paediatric patients with PAH, 4 paediatric healthy controls
Garcia-Alvarez et al[50]	68 ± 22* 59 ± 31#	–	–/−0.54	*Derivation cohort: 80 patients with PH (all groups). #Validation cohort: 20 patients with PH (all groups)
Ley et al[57]	79 ± 26* 66 ± 22#	–	–	10/10 patients with PH (all groups) *with/#without training (here: baseline values)
Rolf et al[53]	61 ± 16* 74 ± 19#	–	–	57 patients with CTEPH *pre- and #post endarterectomy
$v_{mean,avg}$ (cm s^{-1})				
Sanz et al[48]	8.9 ± 2.8	15.6 ± 5.2	−0.73/−0.86	42 patients with PAH, 17 non-PH patients; linear correlation with mPAP and indexed PVR. $AUC_{mPAP>25mmHg} = 0.90$; cut-off = 11.7 cm s^{-1}; sensitivity/specificity = 93%/82%; $AUC_{PVR>3WU} = 0.92$; cut-off = 11.7 cm s^{-1}: sensitivity/specificity = 91%/93%
	16.9 ± 8.7	38.4 ± 16.5	−0.71/−0.78	$v_{mean,avg}$ during AT
	14.6 ± 6.8	29.4 ± 12.4	−0.74/−0.84	$v_{mean,avg}$ during ET
Moral et al[49]	8.9 ± 4.3	14.2 ± 7.1	−0.51/–	152 patients with PH (all groups), 33 non-PH patients; linear correlation with mPAP
Swift et al[15]	7.6 ± 3.4	13.6 ± 6.7	−0.55/−0.56	106 patients with PH (all groups) and non-PH patients; linear correlation with mPAP and PVR. $AUC_{mPAP>25mmHg} = 0.80$; cut-off = 10 cm s^{-1}; sensitivity/specificity = 82%/62%
Ley et al[57]	14 ± 4* 11 ± 2#	–	–	10/10 patients with PH (all groups) *with/#without training (here: baseline values)
Guo et al[55]	7.1 ± 2.5	15.4 ± 3.1	−0.47/−0.62	20 patients with CTEPH, 20 healthy controls. Linear correlation with mPAP and indexed PVR
Helderman et al[51]	16 ± 5	38 ± 10	$R^2 = 0.60$/–	38 patients with PAH, 17 non-PH patients

(Continued)

Table 2. (Continued)

Reference	PH	Non-PH	Correlation mPAP/PVR	Comment
Truong et al[52]	17 ± 11	30 ± 12	–	25 paediatric patients with PAH, 4 paediatric healthy controls. Non-significant difference
	58 ± 34	83 ± 23	–	$V_{mean,avg}$, in systole
Garcia-Alvarez et al[50]	9.7 ± 6.5* 9.1 ± 8.9#	–	–/−0.83	*Derivation cohort: 80 patients with PH (all groups). #Validation cohort: 20 patients with PH (all groups)
Time to v_{peak} (ms)				
Ley et al[27]	98 ± 33	151 ± 27	−0.19/–	22 patients with PAH, 25 healthy controls. Non-significant correlation with mPAP
Ley et al[57]	92 ± 32* 108 ± 61#	–	–	10/10 patients with PH (all groups) *with/#without training (here: baseline values)

4D, four-dimensional; AUC, area under the curve; AT, acceleration time; CTEPH, chronic thromboembolic pulmonary hypertension; ET, ejection time; PAH, pulmonary arterial hypertension; PH, pulmonary hypertension; $v_{mean,avg}$, average mean velocity; v_{peak}, peak velocity.

significantly higher in children with PH than in children without PH and correlated strongly with pulmonary-to-systemic blood pressure ratio in children with PH ($r = 0.90$); the parameters AT, ET, AT/ET, AccV and v_{peak} revealed no significant differences between the PH and non-PH groups.

The blood volume passing the mPA in the cardiac cycle (Q_p) reflects the RVSV, which furthermore can be employed to calculate RVCO by multiplication with heart rate. Both quantities directly correspond to the quantities measured in RHC, and studies with simultaneous PC and RHC data acquisition have indicated satisfactory agreement in patients with PH.[65,66] Discrepancies between methods might occur owing to both limitations of RHC assessment[1,65] and reduced precision of PC imaging in the presence of increased spatial velocity variation.[67–69]

Q_p plays an important role in the evaluation of cardiac shunts, which are a frequent cause of PAH.[70] Without the presence of shunting between the pulmonary and systemic circulation, Q_p equals the systemic blood volume Q_s, and the pulmonary-to-systemic flow ratio $Q_p : Q_s$ should be close to 1. Q_s is typically assessed from an additional 2D PC measurement through the ascending aorta with minimal time delay to the pulmonary flow measurement.[29] Employing velocity offset corrections for both measurements, normal $Q_p : Q_s$ ratios of 1.0 ± 0.1,[37] 1.05 ± 0.07[71] and 0.98 ± 0.11[72] are reported. Current guidelines[2] recommend PC imaging-based assessment of $Q_p : Q_s$ to exclude atrial septal defects and/or anomalous pulmonary venous return in the diagnostic work-up of patients with PH.

Multiparametric models for assessment of pulmonary haemodynamic indices

Different multiparametric models have been introduced to estimate mPAP and PVR from cardiac MR data (Table 4). In a recently published analysis of the diagnostic accuracy levels of cardiac MR and RHC, Wang et al[11] compared 21 MR indices derived in 16 studies (11 *via* PC imaging), which have been reported to reflect the presence of PH. Because of the small number of comparable studies, PC parameters were not summarized in the meta-analysis; therefore, further clinical studies are necessary to confirm the diagnostic value of PC imaging in PH. The validation of the proposed models is challenging, as invasive RHC and MR investigations are typically delayed in time and haemodynamic variations are possible, even in a short time frame.[75]

ADVANCED PC PARAMETERS OF THE PULMONARY ARTERIAL VASCULATURE IN PH

In addition to the derivation of the indices discussed above, 2D and 4D PC imaging allow the derivation of parameters related to blood flow topology, pulse-wave propagation and wall shear stress (WSS) in the pulmonary arterial vasculature. Even though the general applicability of relationships and correlations of MR metrics derived in single-centre studies and well-defined patient groups require further investigation, pre-clinical and clinical studies show promising results in the characterization of PH, even beyond RHC.

Vortical and retrograde blood flow in the main pulmonary artery

Early echocardiographic and PC imaging studies in PH documented a heterogeneous flow profile with substantial middle-to end-systolic retrograde flow (Figure 8a), which was not observed in healthy controls.[61] Employing 4D PC imaging, the origin of this retrograde flow was clarified by Reiter et al,[76] who demonstrated the presence of a vortex of blood flow along the mPA in PH, which does not appear in patients with normal mPAP (Figure 9). The typical rotation direction of the vortex is forward flow at the ventral side of the mPA and backward flow at its dorsal side,[51,76–79] suggesting thickening of the boundary layer and flow separation as the reasons for the onset of vortical flow in PH.[51,76]

The duration of vortical blood flow along the mPA relative to the cardiac interval (t_{vortex}) turned out to be intimately linked to mPAP: Reiter et al[79] proposed a segmented linear model increasing from $t_{vortex} = 0\%$ (below mPAP = 16 mmHg) linearly with a slope of 1.59% per mmHg. This model allowed an accurate estimation of mPAP with a standard deviation of 3.9 mmHg, regardless of the PH group. Moreover, the model-based cut-off value for 25 mmHg ($t_{vortex} = 14.3\%$) revealed a high diagnostic accuracy for identifying

Table 3. Parameters derived from the time course of the main pulmonary artery blood flow obtained from MR phase-contrast measurements and their correlation to the main pulmonary arterial pressure (mPAP) and pulmonary vascular resistance (PVR)

Reference	PH	non-PH	Correlation mPAP/PVR	Comment
Q_{max} (ml s^{-1})				
Barker et al[56]	277 ± 73	337 ± 72		10 patients with PAH, 9 healthy controls (2 centres). Evaluation from 4D PC imaging
Q_{mean} (ml s^{-1})				
Guo et al[55]	74 ± 20	73 ± 18	−0.38/−0.73	20 patients with CTEPH, 20 healthy controls. Linear correlation with indexed PVR
Ley et al[54]	35 ± 13* 47 ± 17#	67 ± 20	–	35 patients with CTEPH (*pre- and #post pulmonary thromboendarterectomy), 10 healthy controls
Ley et al[27]	82 ± 23	107 ± 25	–	22 patients with PAH, 25 healthy controls
Truong et al[52]	40 ± 16	43 ± 20	–	25 paediatric patients with PAH, 4 paediatric healthy controls. Non-significant difference
Ley et al[57]	95 ± 20* 85 ± 23#	–		10/10 patients with PH (all groups) *with/#without training (here: baseline values)
Relative RF (%)				
Kondo et al[61]	17 ± 14	3 ± 2	0.20/0.48	10 patients with PH (all groups), 10 non-PH patients. Non-significant correlation with mPAP. Natural logarithm of RF: correlation with mPAP/PVR = 0.48/0.63
Helderman et al[51]	9 ± 5	1 ± 1	R^2 = 0.54/–	38 patients with PAH, 17 non-PH patients
Swift et al[15]	16 ± 9	9 ± 7	0.34/0.31	106 patients with PH (all groups) and non-PH patients; linear correlation with mPAP and PVR. $AUC_{mPAP>25mmHg}$ = 0.75
AccV (ml)				
Mousseaux et al[62]	15 ± 5	29 ± 8# 42 ± 12*	–/−0.78	12 patients with PH (all groups),#7 non-PH patients,*10 healthy controls
Maximal dQ/dt_{max} (ml s^{-2})				
Mousseaux et al[62]	6.77 ± 1.80	6.59 ± 1.05# 7.18 ± 2.72*	–	12 patients with PH (all groups),#7 non-PH patients,*10 healthy controls
AT (ms)				
Mousseaux et al[62]	87 ± 24	128 ± 23# 134 ± 19*	–/−0.65	12 patients with PH (all groups),#7 non-PH patients,*10 healthy controls
Sanz et al[48]	128 ± 26	146 ± 22	−0.35/−0.35	42 patients with PAH, 10 healthy controls; linear correlation with mPAP and indexed PVR
Helderman et al[51]	89 ± 29	107 ± 20	–	38 patients with PAH, 17 non-PH patients
Alunni et al[25]	127 ± 34		–/−0.50	37 patients with PH
ET (ms)				
Sanz et al[48]	383 ± 77	393 ± 74	−0.17/−0.19	42 patients with PAH, 10 healthy controls; non-significant correlations with mPAP and indexed PVR
Alunni et al[25]	322 ± 60	–	–	37 patients with PH

(Continued)

Table 3. (Continued)

Reference	PH	non-PH	Correlation mPAP/PVR	Comment
AT/ET (ms)				
Sanz et al[48]	0.34 ± 0.08	0.37 ± 0.08	−0.28/−0.29	42 patients with PAH, 17 non-PH patients; linear correlation with mPAP and indexed PVR
Helderman et al[51]	0.29 ± 0.07	0.34 ± 0.07	–	38 patients with PAH, 17 non-PH patients
Rolf et al[53]	0.32 ± 0.06* 0.36 ± 0.09#	–	–	57 patients with CTEPH *pre- and #post endarterectomy
rROT (%)				
Helderman et al[51]	14 ± 6	37 ± 6	$R^2 = 0.62$/–	38 patients with PAH, 17 non-PH patients. rROT >25%; sensitivity/specificity = 100%/100%

4D, four-dimensional; AccV, acceleration volume; AUC, area under the curve; AT, acceleration time; CTEPH, chronic thromboembolic pulmonary hypertension; dQ/dt_{max}, maximum change in flow rate during ejection; ET, ejection time; PAH, pulmonary arterial hypertension; PH, pulmonary hypertension; Q_{max}, maximal blood flow; Q_{mean}, mean blood flow; RF, retrograde blood flow; rROT, relative onset of retrograde flow.

PH (sensitivity/specificity, 97%/96%). t_{vortex}, originally determined by visual inspection of vector plots,[76,79] might be similarly derived from streamline or particle trace visualizations.[80] Spatial three-dimensional information especially facilitates the discrimination of circular (vortical) motion along the mPA from helical (spiralling) blood flow into the right pulmonary artery (Figure 10), frequently occurring without the presence of elevated mPAP.[81,82]

Helderman et al[51] studied the relative onset time of retrograde flow (rROT) by segmentation of the backward flow component in 2D PC measurements in the mPA (Figure 8). Compatible with a close relationship between vortex duration and mPAP, a strong linear correlation between rROT and mPAP ($r^2 = 0.62$) was found in patients with PAH and non-PH subjects. Moreover, the cut-off rROT = 25% distinguished patients with PAH from non-PH subjects (sensitivity/specificity, 100%/100%). Interestingly, flow volume-related parameters of the retrograde flow (Table 3) revealed weaker correlations with mPAP and PVR.[15,51]

Pulse-wave velocity

Blood ejected from the right ventricle generates a pressure or flow wave, which propagates through the pulmonary vasculature with pulse-wave velocity (PWV). An increase of PWV is directly related to a decrease of compliance and distensibility of the pulmonary vasculature,[29] which in turn is an early sign of PH.[83]

Two methods have been introduced to estimate pulmonary arterial PWV from PC imaging: (1) the transit-time (TT) approach (Figure 11a) derives PWV from the TT of the flow wave between two levels in the pulmonary vascular tree (generically, the pulmonary trunk and the proximal left or right pulmonary artery) and the distance between these localizations.[84] (2) The flow area (QA) method (Figure 11b) equates PWV with the linear increase of flow with respect to the pulmonary artery vessel cross-sectional area during early systole.[85] Both methods benefit from a high temporal resolution of the employed PC sequences: the TT approach because of the short distances between measurement positions in the pulmonary artery and the QA approach owing to the more reliable linear fitting. The necessity of an accurate assessment of the cross-sectional area changes suggests in addition an adequate spatial resolution of the PC imaging sequence in the QA approach.[86]

Comparing the two techniques, Ibrahim et al[86] found good agreement of PWVs determined by TT and QA approaches ($r = 0.94$) without any significant bias. PWV in the pulmonary artery almost doubled in the studied PAH group ($5.2 \pm 0.5\ m\ s^{-1}$) compared with patients with cardiovascular disease without known PH ($2.8 \pm 0.9\ m\ s^{-1}$). Taking into account age differences and the presence of cardiovascular disease, the pulmonary arterial PWV of patients without known PH compared well with the normal values found by Peng et al[85] ($1.8 \pm 0.3\ m\ s^{-1}$ by QA approach) and Bradlow et al[84] (2.1 ± 0.6 and $2.3 \pm 0.4\ m\ s^{-1}$ employing TT approach between the mPA and the proximal left or right pulmonary artery, respectively).

Quail et al[63] derived substantially lower PWVs in the pulmonary artery by the QA approach, which possibly might be explained by differences in the time resolution of the employed PC imaging protocols or duration of the early systolic phase used for fitting. However, PWVs in the main, proximal left and proximal right pulmonary arteries were again approximately doubled in patients with PH compared with age-matched healthy volunteers. By extending the analysis of the relationship between the flow and cross-sectional area, Quail et al[63] were moreover able to demonstrate the altered wave reflection behaviour present in PH.[53,58]

Wall shear stress

As suggested by the studies employing computational fluid dynamics,[87,88] the chronic elevation of mPAP in PH affects the viscous haemodynamic forces to the vessel walls of the pulmonary vasculature. These forces, measured by WSS, are important determinants of endothelial cell function and gene expression;[88] PC imaging possesses the potential for their estimation in the proximal pulmonary vasculature.

Table 4. Multiparametric models to estimate the main pulmonary arterial pressure (mPAP) and pulmonary vascular resistance (PVR) employing parameters derived from through-plane two-dimensional MR phase-contrast measurements

Reference	Model	Correlation with RHC	Comment
García-Álvarez et al[50]	$PVR_{MR} = 19.38 - (4.62 \times \ln v_{mean,avg}) - (0.08 \times RVEF)$	$r = 0.84$* $r = 0.84$#	*Derivation cohort: 80 patients with PH (all groups). #Validation cohort: 20 patients with PH (all groups). $AUC_{PVR>3WU} = 0.96$; PVR_{MR} cut-off value of 11.7; sensitivity/specificity = 93%/85%
Kreitner et al[66]	$mPAP_{MR} = 69.446 - 0.521 \times AT - 0.570 \times v_{mean,max} + 1.507 \times AccV + 0.002 \times (dQ/dt)_{max}$	$R^2 = 0.89$	19 patients with CTEPH
	$PVR_{MR} = (mPAP_{MR} - 10)/RVCO$	$R^2 = 0.79$	
Bane et al[73]	$mPAP_{MR} = -2.3 + 1.06 \times RVEDV/RVEF$	$R^2 = 0.46$	7 patients with PH.
	$PVR_{MR} = mPAP_{MR} - (1.9 + 0.77 \times E/e')/RVCO$		
Moral et al[49]	$mPAP \propto \alpha = A_{min}/RVEF$	$r = 0.61$	152 patients with PH (all groups), 33 non-PH patients. $AUC_{mPAP\geq25} = 0.95$; cut-off value $\alpha = 7.2$; sensitivity/specificity = 90%/88%
Laffon et al[74]	$mPAP = v_{peak}\ (cm\,s^{-1})^{0.5} \times height\ (m)^{-0.83} \times weight\ (kg)^{-0.3} \times HR\ (min^{-1})^{-0.14} + A_{max}\ (cm^2)^{1.5} \times height\ (m)^{-4.3} \times weight\ (kg)^{-2.3} \times HR\ (min^{-1})^{0.6}$	$r = 0.92$	31 patients with PH (all groups)
Mousseaux et al[62]	$mPAP_{MR} = -4.6 + (IVSA \times 0.23) + (VMI \times 16.3)$	$R^2 = 0.75$* $R^2 = 0.67$#	12 patients with PH (all groups), 7 non-PH patients, 10 healthy controls. IVSA; VMI
Swift et al[21]	$PAWP_{MR} = 6.43 + LAVI \times 0.22$	$R^2 = 0.36$* $R^2 = 0.49$#	*Derivation cohort: 64 patients with PH (all groups). #Validation cohort: 66 patients with PH (all groups).
	$PVR_{MR} = (mPAP_{MR} - PAWP_{MR})/RVCO$	$R^2 = 0.67$* $R^2 = 0.76$#	
	$mPAP_{MR} = -4.6 + (IVSA \times 0.23) + (VMI \times 16.3)$	$R^2 = 0.75$* $R^2 = 0.67$#	

AccV, acceleration volume; A_{min}, minimal cross-sectional area; AUC, area under the curve; AT, acceleration time; CTEPH, chronic thromboembolic pulmonary hypertension; dQ/dt_{max}, maximum change in flow rate during ejection; E, early diastolic mitral peak velocity; e', early diastolic tissue peak velocity; HR, heart rate; IVSA, intraventricular septum angle; LAVI, left atrial volume index; ln $v_{mean,avg}$, natural logarithm of average mean velocity; PAWP, pulmonary arterial wedge pressure; PH, pulmonary hypertension; RHC, right heart catheterization; RVCO, right ventricular cardiac output; RVEDV, right ventricular end-diastolic volume; RVEF, right ventricular ejection fraction; VMI, ventricular mass index; $v_{mean,max}$, maximum mean velocity; v_{peak}, peak velocity.

WSS is defined as the tangential force per unit area that is exerted by blood flow to the surface of the vessel. Assuming blood flow along the vessel, the magnitude of WSS is proportional to the radial velocity gradient at the vessel wall (Figure 12); the proportionality factor is the viscosity of blood (η_{blood}). Accordingly, a through-plane 2D PC measurement perpendicular to a vessel allows the estimation of the (time course of) WSS experienced by the vessel wall from determination of (the time course of) the radial velocity gradients at the vessel wall and from an assumption about the magnitude of η_{blood} (typically, η_{blood} is chosen independent of the subject in the range $3–4 \times 10^{-3}$ Pa s^{-1}).[52,88,89] Aside from the general advantage of *a posteriori* choice of cross-sections, 4D PC measurement enables the additional estimation of the circumferential component of WSS in the presence of secondary in-plane blood flow.[56,90]

In accordance with computational fluid dynamics results,[87] PC imaging-derived WSS in the proximal pulmonary vasculature was found to be reduced in PH (owing to the limited spatial resolution, as expected,[32,90] absolute PC imaging-derived WSS values were smaller): Truong et al[52] investigated WSS in the right pulmonary artery in a paediatric PAH population employing 2D PC imaging and demonstrated significant decreases of circumferentially and time-averaged WSS (0.22 ± 0.16 N m^{-2} *vs* 0.66 ± 0.34 N m^{-2}) and circumferentially averaged systolic WSS (0.8 ± 0.5 N m^{-2} *vs* 2.0 ± 0.9 N m^{-2}) in patients with PAH compared with healthy controls. Moreover, Truong et al[52] showed that even if pulmonary net flow rates are preserved, vessel dilatation in PAH results in lower velocity gradients at the vessel wall, and thus lower WSS. In a recent study, Barker et al[56] calculated WSS in the main, left and right pulmonary arteries of adult patients with PH from 4D PC measurements. In accordance with the above 2D PC imaging study, decreased magnitude of circumferentially and time-averaged WSS was found in PH in the main (PH, 0.22 ± 0.10 N m^{-2}; healthy controls, 0.40 ± 0.14 N m^{-2}), left

Figure 8. Retrograde blood flow (RF) in a through-plane two-dimensional phase-contrast measurement in the main pulmonary artery (mPA) of a patient with pulmonary arterial hypertension (a). Onset time (ROT) of RF as well as the relative onset time of retrograde flow (rROT) with respect to cardiac interval (RR) can be evaluated by segmentation of RF in the velocity images (b).

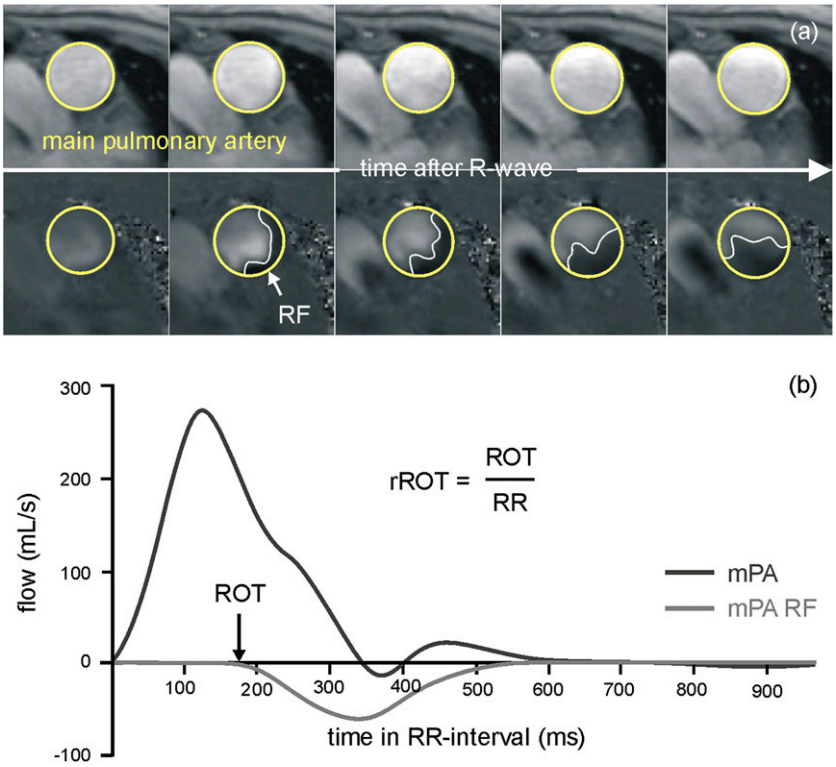

(PH, $0.16 \pm 0.09\,N\,m^{-2}$; healthy controls, $0.41 \pm 0.18\,N\,m^{-2}$) and right pulmonary artery (PH, $0.19 \pm 0.07\,N\,m^{-2}$; healthy controls, $0.54 \pm 0.21\,N\,m^{-2}$). Furthermore, the relative contributions of circumferential WSS to the magnitude of WSS were increased in PH in the main (PH, 15%; healthy controls, 6%) as well as left pulmonary artery (PH, 14%; healthy controls, 9%) but not in the right pulmonary branch (PH and healthy controls, 15%), which is in accordance with the observed vortical blood flow in

Figure 9. Vector plots of mid-systolic blood flow velocity fields in a healthy volunteer (a) and a patient with pulmonary hypertension (PH) (b) in orientation of the right ventricular outflow tract. Whereas blood motion is uniformly directed forward in the main pulmonary artery of the healthy volunteer, a vortical blood flow pattern along the main pulmonary artery is observed in the main pulmonary artery in the patient with PH.

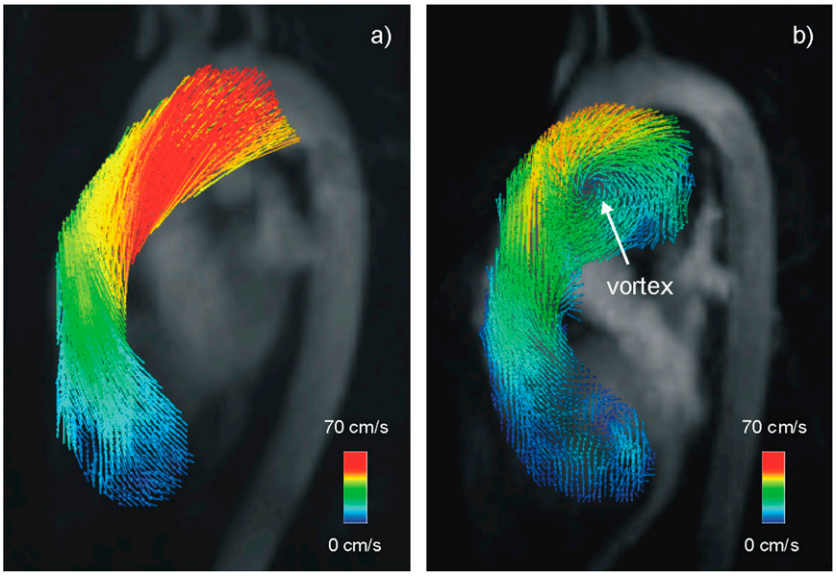

Figure 10. Early diastolic streamline visualizations of main pulmonary artery blood flow in two different patients with pulmonary arterial hypertension. A parallel appearance of vortical flow in the main pulmonary artery and helical flow into the right pulmonary artery (a). Pulmonary regurgitation does not hinder formation of vortical blood flow (b).

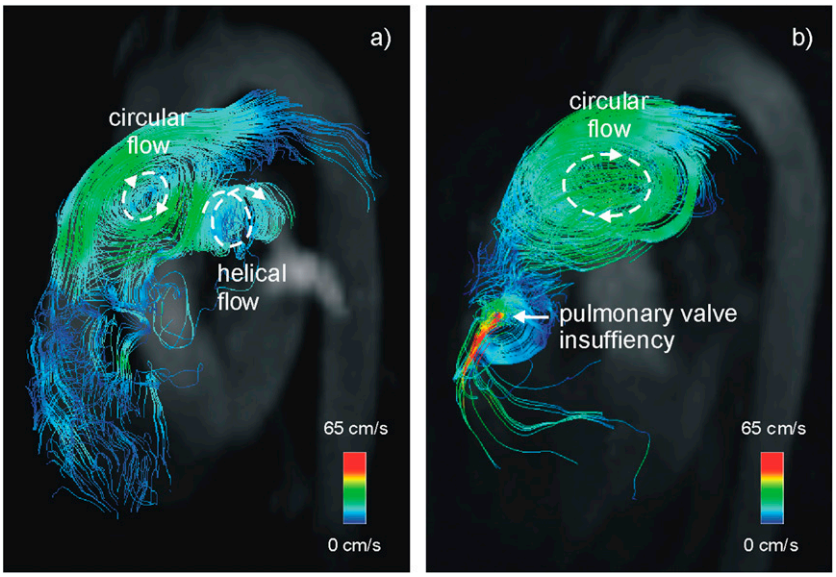

PH[43,51,76–79] and the helical blood flow into the right pulmonary artery frequently found without the presence of elevated mPAP.[81,82]

PHASE-CONTRAST INDICES OF VENTRICULAR FUNCTION

As indicated in Figure 1, PH is not a single disease of the pulmonary artery but rather a condition that progressively impairs the pulmonary circulation and causes right heart failure, which represents the major cause of mortality from PH.[1,91] Therefore, besides analysis of the pulmonary vasculature, evaluation of the right ventricular performance is of central relevance for the evaluation and characterization of PH.[47,91]

Tricuspid regurgitation

PH is a common cause for tricuspid regurgitation, which is an independent risk factor for mortality in general and in patients with PH.[92] Not all patients with PH develop severe tricuspid regurgitation; quantification of tricuspid regurgitation volume and regurgitation fraction (regurgitation volume as a percentage of the total transvalvular blood volume) is, however, important for patient management. As described above, PC imaging enables the quantification of blood volumes through arbitrary tomographic slice positions, and therefore also through intracardiac valves. The continuous translation of the valvular plane with the contraction and relaxation of the heart, on the other hand, makes it

Figure 11. Assessment of pulse-wave velocity (PWV) in the pulmonary artery by transit-time approach (a) and flow-area method (b). Δx denotes the distance between measurement positions, Δt is difference of velocity onsets. Black dots in the vessel area—flow plot display measured data points in early systole. RR, cardiac interval.

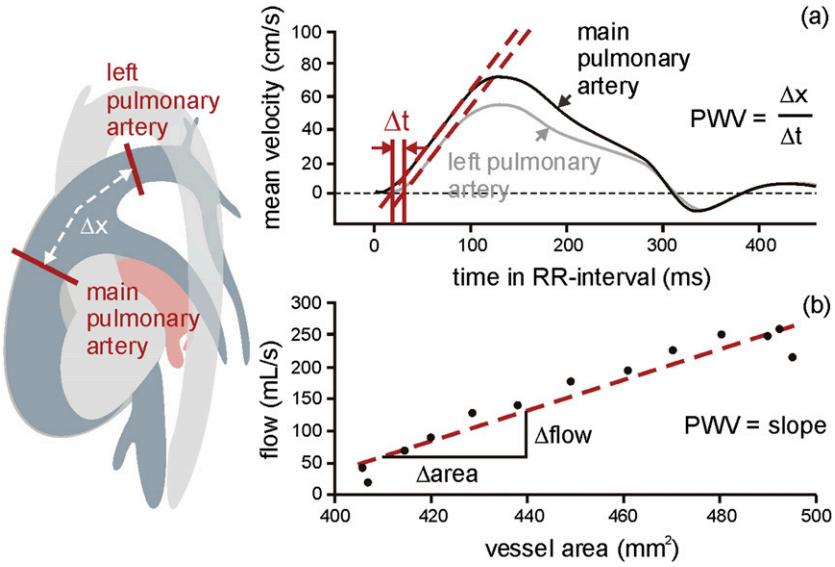

Figure 12. Schematic drawing illustrating the definition of wall shear stress (WSS). $\Delta v/\Delta x$ denotes the radial velocity gradient at the vessel wall. η_{blood} is the viscosity of blood.

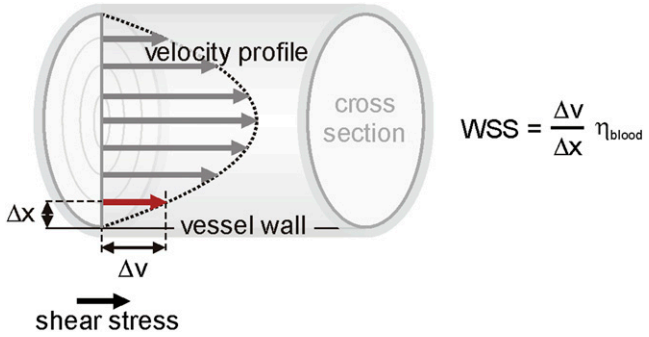

challenging to assess the time courses of blood flow and its velocities through the tricuspid valve from static 2D PC imaging slice positions.

Tricuspid inflow velocities are commonly determined from a through-plane 2D PC measurement, with the acquisition plane aligned parallel to the valvular plane in early diastole, slightly shifted to the ventricular side of the valve (Figure 13a). In contrast to the evaluation of blood flow through a vessel cross-section, the segmentation of transvalvular blood flow may be easier on velocity (phase) images than on magnitude images (Figure 13b). In line with findings from echocardiographic studies, PC imaging-derived early (E-wave) and late (A-wave) diastolic tricuspid and mitral peak velocities, as well as the time delay between tricuspid and mitral E-waves, have been shown to be significantly associated with the sPAP and PVR in PH.[25] Westenberg et al[93] demonstrated that the assessment of tricuspid flow and regurgitation volumes from 4D PC data with retrospective manual alignment of multiplanar reconstructed tricuspid valvular imaging planes enables more accurate quantification of tricuspid flow volume, regurgitation volume and regurgitation fraction than does the use of 2D PC imaging. Roess et al[94] and Hsiao et al[95] analyzed flow and regurgitation volumes through all cardiac valves in healthy controls and patients with diverse valvular and shunt pathologies and found highly consistent results.

In addition to the quantification of regurgitation volumes, the measurement of regurgitation jet peak velocity—as typically assessed by echocardiography to estimate systolic pressure from the modified Bernoulli equation ($sPAP = 4 \times v_{peak}^2 + RAP$; sPAP and RAP in mmHg, v_{peak} in m s^{-1})—is also feasible with through-plane 2D PC imaging.[96] To determine jet peak velocity, the acquisition plane must be angulated perpendicular to the valvular jet flow (Figure 13c,d), ideally positioned at the level of the vena contracta. Comparing the sPAP derived from PC imaging regurgitation jet peak velocity with that of RHC in patients with suspected PH, Nogami et al[96] demonstrated a high correlation ($r = 0.94$) and a slight underestimation (−3.2 mmHg) of PC imaging-derived sPAP (RAP was assumed to be 10 mmHg in all subjects).

Right ventricular function and kinetic energy

Right heart dysfunction is a strong predictor of adverse clinical outcome in PH. Therefore, accurate evaluation of right ventricular function is an important part of clinical staging of patients with PH. Cardiac MR is the established reference standard for the assessment of systolic ventricular function and ventricular mass from cine steady-state free-precession (SSFP) imaging using the Simpson approach.[8,9] Providing time-resolved magnitude images, 4D PC data can be used to evaluate the indices of right ventricular systolic function from volume segmentation; Hsiao et al[95] found excellent correlations between this approach and standard cine SSFP imaging.

Beyond the assessment of standard parameters of right ventricular function, 4D PC imaging allows energy analysis of the right ventricle based on the fact that kinetic energy of a voxel is given by $m_{voxel} \times v_{voxel}^2/2$, where v_{voxel} denotes the measured magnitude of the three-directional velocity in the voxel; voxel mass m_{voxel} can be determined from its volume and an average density of blood. Time courses of kinetic energy of the right ventricular blood or kinetic energies related to volumetric components (for example, the volumetric component that enters and leaves the right ventricle directly during one heart beat) may be calculated.[97,98] Furthermore, in the sense of an energy balance, right ventricular kinetic energy work can be introduced by subtracting the kinetic energy portion entering the right ventricle through the tricuspid and the pulmonic valve from the kinetic energy portion leaving the right ventricle through the tricuspid and the pulmonic valve. Although neglecting tricuspid regurgitation, Han et al[99] recently found significantly higher right ventricular kinetic energy work density (defined as kinetic energy work-divided right ventricular stroke volume) in patients with PH (94.7 ± 33.7 mJ ml^{-1}) compared with healthy subjects (61.7 ± 14.8 mJ ml^{-1}). The increase in right ventricular kinetic energy work density in PH was attributed to altered diastolic right ventricular vortex formation, which was independently documented by Fenster et al.[100] Han et al[99] furthermore quantified the viscous energy dissipation in the mPA with respect to the kinetic energy output of the right ventricle and found a significant increase in patients with PH ($21.1 \pm 6.4\%$) compared with healthy controls ($2.2 \pm 1.3\%$), which could be related to the vortical blood flow patterns[43,51,76–79] described above.

CONCLUSION

The present review demonstrates the enormous potential of MR PC imaging in the evaluation of PH. At present, the major limitations of an integrated PC imaging pathway in PH are that cardiac MR in general is time consuming, expensive, not widely available and requires operator expertise. Through-plane 2D PC imaging in the mPA represents a standard technique and is recommended in patients in whom PH is suspected.[2,101,102] Even though various standard parameters derived from the technique have a high predictive value for the identification of PH, elevated pulmonary arterial pressures and PVR cannot be excluded based on these measurements; multiparametric models including these parameters need further evaluation of their applicability. Non-standard metrics derived from the measurement in the mPA or from further through-plane 2D PC acquisitions (as PWV, WSS, rROT, tricuspid inflow profile and regurgitation jet peak velocity) might add additional information to characterize PH. Future larger scale

Figure 13. Planning of the through-plane two-dimensional phase-contrast imaging acquisition plane of tricuspid inflow (solid line) on early diastolic images in 4-chamber (left) and right ventricular 2-chamber (right) view (a) and delineation of the tricuspid inflow (yellow region of interest) on resulting magnitude (left) and velocity (right) images (b). Planning of the tricuspid regurgitation jet velocity on systolic images in 4-chamber (left) and right ventricular 2-chamber (right) view (c) and determination of the peak velocity (v_{peak}) (d). (Acquisition plane 1 cm proximal to the tricuspid valve[96]). VENC, velocity-encoding value.

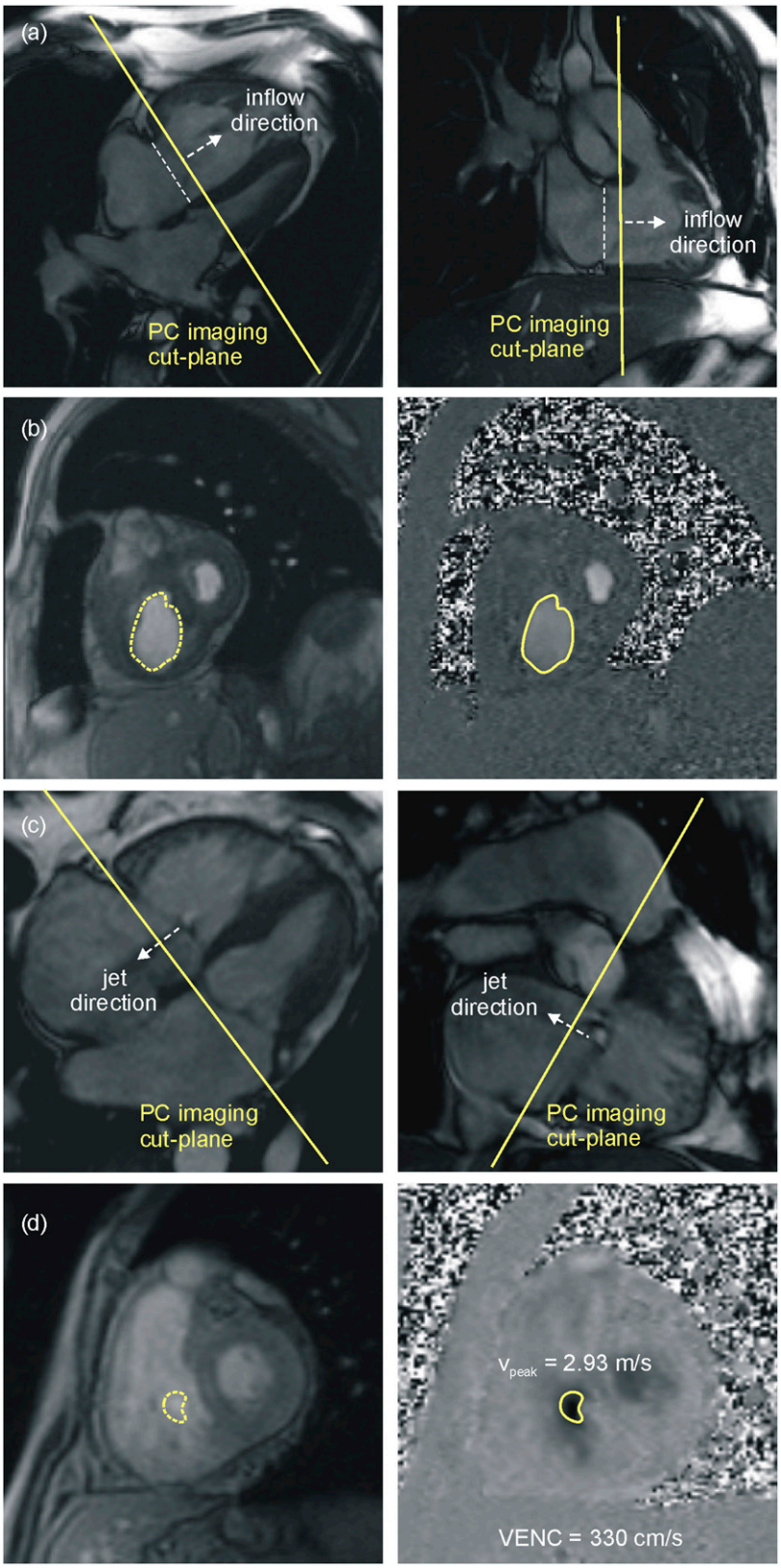

and multicentre cohort studies will have to show the potential diagnostic and/or prognostic benefits of multiparametric models and non-standard measures, respectively. 4D PC imaging and the fluid mechanical variables it provides are the subjects of active research.[30–33] Both, 4D PC imaging sequences and post-processing software are still pre-product developments and therefore not available for clinical routine. Preliminary results indicate that parameters directly related to RHC haemodynamic indices (such as the vortex of blood flow in the mPA) as well as metrics not available from routine RHC (such as WSS and kinetic energy losses) have great potential for non-invasive PH screening and monitoring. It is to be expected that 4D PC imaging will provide further key metrics for the assessment of PH, especially for the assessment of left atrial and ventricular function;[32,103] the latter are important not only in the large group of patients whose PH is due to left heart disease, but also in patients with PH in general.

ACKNOWLEDGMENTS

Gert Reiter is employed by Siemens Healthcare. All authors have declared that no competing interests exist. The authors thank Ada Muellner, MS, for editing the manuscript.

FUNDING

This work was supported by the funds of the Oesterreichische Nationalbank, Anniversary Fund (grant number 141223) and the Styrian Government, Department 8 for Science and Research (grant number A3-16.R-8/2012-8).

REFERENCES

1. Hoeper MM, Bogaard HJ, Condliffe R, Frantz R, Khanna D, Kurzyna M, et al. Definitions and diagnosis of pulmonary hypertension. *J Am Coll Cardiol* 2013; **62** (Suppl. 25): D42–50. doi: http://dx.doi.org/10.1016/j.jacc.2013.10.032
2. Galiè N, Humbert M, Vachiery JL, Gibbs S, Lang I, Torbicki A, et al. 2015 ESC/ERS Guidelines for the diagnosis and treatment of pulmonary hypertension: The Joint Task Force for the Diagnosis and Treatment of Pulmonary Hypertension of the European Society of Cardiology (ESC) and the European Respiratory Society (ERS): Endorsed by: Association for European Paediatric and Congenital Cardiology (AEPC), International Society for Heart and Lung Transplantation (ISHLT). *Eur Respir J* 2015; **46**: 903–75. doi: http://dx.doi.org/10.1183/13993003.01032-2015
3. Simonneau G, Gatzoulis MA, Adatia I, Celermajer D, Denton C, Ghofrani A, et al. Updated clinical classification of pulmonary hypertension. *J Am Coll Cardiol* 2013; **62** (Suppl. 25): D34–41. doi: http://dx.doi.org/10.1016/j.jacc.2013.10.029
4. Pawade T, Holloway B, Bradlow W, Steeds RP. Noninvasive imaging for the diagnosis and prognosis of pulmonary hypertension. *Expert Rev Cardiovasc Ther* 2014; **12**: 71–86. doi: http://dx.doi.org/10.1586/14779072.2014.867806
5. Vonk Noordegraaf A, Haddad F, Bogaard HJ, Hassoun PM. Noninvasive imaging in the assessment of the cardiopulmonary vascular unit. *Circulation* 2015; **131**: 899–913. doi: http://dx.doi.org/10.1161/CIRCULATIONAHA.114.006972
6. Kreitner KF. Noninvasive imaging of pulmonary hypertension. *Semin Respir Crit Care Med* 2014; **35**: 99–111. doi: http://dx.doi.org/10.1055/s-0033-1363456
7. Naeije R, D'Alto M, Forfia PR. Clinical and research measurement techniques of the pulmonary circulation: the present and the future. *Prog Cardiovasc Dis* 2015; **57**: 463–72. doi: http://dx.doi.org/10.1016/j.pcad.2014.12.003
8. Kramer CM, Barkhausen J, Flamm SD, Kim RJ, Nagel E; Society for Cardiovascular Magnetic Resonance Board of Trustees Task Force on Standardized Protocols. Standardized cardiovascular magnetic resonance (CMR) protocols 2013 update. *J Cardiovasc Magn Reson* 2013; **15**: 91. doi: http://dx.doi.org/10.1186/1532-429X-15-91
9. Schulz-Menger J, Bluemke DA, Bremerich J, Flamm SD, Fogel MA, Friedrich MG, et al. Standardized image interpretation and post processing in cardiovascular magnetic resonance: Society for Cardiovascular Magnetic Resonance (SCMR) board of trustees task force on standardized post processing. *J Cardiovasc Magn Reson* 2013; **15**: 35. doi: http://dx.doi.org/10.1186/1532-429X-15-35
10. Swift AJ, Wild JM, Nagle SK, Roldán-Alzate A, François CJ, Fain S, et al. Quantitative magnetic resonance imaging of pulmonary hypertension: a practical approach to the current state of the art. *J Thorac Imaging* 2014; **29**: 68–79. doi: http://dx.doi.org/10.1097/RTI.0000000000000079
11. Wang N, Hu X, Liu C, Ali B, Guo X, Liu M, et al. A systematic review of the diagnostic accuracy of cardiovascular magnetic resonance for pulmonary hypertension. *Can J Cardiol* 2014; **30**: 455–63. doi: http://dx.doi.org/10.1016/j.cjca.2013.11.028
12. Iwasawa T. Diagnosis and management of pulmonary arterial hypertension using MR imaging. *Magn Reson Med Sci* 2013; **12**: 1–9. doi: http://dx.doi.org/10.2463/mrms.2012-0040
13. Marrone G, Mamone G, Luca A, Vitulo P, Bertani A, Pilato M, et al. The role of 1.5T cardiac MRI in the diagnosis, prognosis and management of pulmonary arterial hypertension. *Int J Cardiovasc Imaging* 2010; **26**: 665–81. doi: http://dx.doi.org/10.1007/s10554-010-9623-2
14. McLure LE, Peacock AJ. Cardiac magnetic resonance imaging for the assessment of the heart and pulmonary circulation in pulmonary hypertension. *Eur Respir J* 2009; **33**: 1454–66. doi: http://dx.doi.org/10.1183/09031936.00139907
15. Swift AJ, Rajaram S, Condliffe R, Capener D, Hurdman J, Elliot CA, et al. Diagnostic accuracy of cardiovascular magnetic resonance imaging of right ventricular morphology and function in the assessment of suspected pulmonary hypertension results from the ASPIRE registry. *J Cardiovasc Magn Reson* 2012; **14**: 40. doi: http://dx.doi.org/10.1186/1532-429X-14-40
16. Roeleveld RJ, Marcus JT, Boonstra A, Postmus PE, Marques KM, Bronzwaer JG, et al. A comparison of noninvasive MRI-based methods of estimating pulmonary artery pressure in pulmonary hypertension. *J Magn Reson Imaging* 2005; **22**: 67–72. doi: http://dx.doi.org/10.1002/jmri.20338
17. Dellegrottaglie S, Sanz J, Poon M, Viles-Gonzalez JF, Sulica R, Goyenechea M, et al. Pulmonary hypertension: accuracy of detection with left ventricular septal-to-free wall curvature ratio measured at cardiac MR. *Radiology* 2007; **243**: 63–9. doi:

http://dx.doi.org/10.1148/radiol.2431060067
18. Sato T, Tsujino I, Ohira H, Oyama-Manabe N, Ito YM, Noguchi T, et al. Paradoxical interventricular septal motion as a major determinant of late gadolinium enhancement in ventricular insertion points in pulmonary hypertension. *PLoS One* 2013; **8**: e66724. doi: http://dx.doi.org/10.1371/journal.pone.0066724
19. Freed BH, Gomberg-Maitland M, Chandra S, Mor-Avi V, Rich S, Archer SL, et al. Late gadolinium enhancement cardiovascular magnetic resonance predicts clinical worsening in patients with pulmonary hypertension. *J Cardiovasc Magn Reson* 2012; **14**: 11. doi: http://dx.doi.org/10.1186/1532-429X-14-11
20. Junqueira FP, Macedo R, Coutinho AC, Loureiro R, De Pontes PV, Domingues RC, et al. Myocardial delayed enhancement in patients with pulmonary hypertension and right ventricular failure: evaluation by cardiac MRI. *Br J Radiol* 2009; **82**: 821–6. doi: http://dx.doi.org/10.1259/bjr/28241773
21. Swift AJ, Rajaram S, Hurdman J, Hill C, Davies C, Sproson TW, et al. Noninvasive estimation of PA pressure, flow, and resistance with CMR imaging: derivation and prospective validation study from the ASPIRE registry. *JACC Cardiovasc Imaging* 2013; **6**: 1036–47. doi: http://dx.doi.org/10.1016/j.jcmg.2013.01.013
22. Jardim C, Rochitte CE, Humbert M, Rubenfeld G, Jasinowodolinski D, Carvalho CR, et al. Pulmonary artery distensibility in pulmonary arterial hypertension: an MRI pilot study. *Eur Respir J* 2007; **29**: 476–81. doi: http://dx.doi.org/10.1183/09031936.00016806
23. Gan CT, Lankhaar JW, Westerhof N, Marcus JT, Becker A, Twisk JW, et al. Noninvasively assessed pulmonary artery stiffness predicts mortality in pulmonary arterial hypertension. *Chest* 2007; **132**: 1906–12. doi: http://dx.doi.org/10.1378/chest.07-1246
24. Shehata ML, Harouni AA, Skrok J, Basha TA, Boyce D, Lechtzin N, et al. Regional and global biventricular function in pulmonary arterial hypertension: a cardiac MR imaging study. *Radiology* 2013; **266**: 114–22. doi: http://dx.doi.org/10.1148/radiol.12111599
25. Alunni JP, Degano B, Arnaud C, Tétu L, Blot-Soulétie N, Didier A, et al. Cardiac MRI in pulmonary artery hypertension: correlations between morphological and functional parameters and invasive measurements. *Eur Radiol* 2010; **20**: 1149–59. doi: http://dx.doi.org/10.1007/s00330-009-1664-3
26. Srichai MB, Lim RP, Wong S, Lee VS. Cardiovascular applications of phase-contrast MRI. *AJR Am J Roentgenol* 2009; **192**: 662–75. doi: http://dx.doi.org/10.2214/AJR.07.3744
27. Ley S, Mereles D, Puderbach M, Gruenig E, Schöck H, Eichinger M, et al. Value of MR phase-contrast flow measurements for functional assessment of pulmonary arterial hypertension. *Eur Radiol* 2007; **17**: 1892–7. doi: http://dx.doi.org/10.1007/s00330-006-0559-9
28. Gatehouse PD, Keegan J, Crowe LA, Masood S, Mohiaddin RH, Kreitner KF, et al. Applications of phase-contrast flow and velocity imaging in cardiovascular MRI. *Eur Radiol* 2005; **15**: 2172–84. doi: http://dx.doi.org/10.1007/s00330-005-2829-3
29. Nayak KS, Nielsen JF, Bernstein MA, Markl M, D Gatehouse P, M Botnar R, et al. Cardiovascular magnetic resonance phase contrast imaging. *J Cardiovasc Magn Reson* 2015; **17**: 71. doi: http://dx.doi.org/10.1186/s12968-015-0172-7
30. Markl M, Kilner PJ, Ebbers T. Comprehensive 4D velocity mapping of the heart and great vessels by cardiovascular magnetic resonance. *J Cardiovasc Magn Reson* 2011; **13**: 7. doi: http://dx.doi.org/10.1186/1532-429X-13-7
31. Markl M, Frydrychowicz A, Kozerke S, Hope M, Wieben O. 4D flow MRI. *J Magn Reson Imaging* 2012; **36**: 1015–36. doi: http://dx.doi.org/10.1002/jmri.23632
32. Hope MD, Sedlic T, Dyverfeldt P. Cardiothoracic magnetic resonance flow imaging. *J Thorac Imaging* 2013; **28**: 217–30. doi: http://dx.doi.org/10.1097/RTI.0b013e31829192a1
33. Dyverfeldt P, Bissell M, Barker AJ, Bolger AF, Carlhäll CJ, Ebbers T, et al. 4D flow cardiovascular magnetic resonance consensus statement. *J Cardiovasc Magn Reson* 2015; **17**: 72. doi: http://dx.doi.org/10.1186/s12968-015-0174-5
34. Fratz S, Chung T, Greil GF, Samyn MM, Taylor AM, Valsangiacomo Buechel ER, et al. Guidelines and protocols for cardiovascular magnetic resonance in children and adults with congenital heart disease: SCMR expert consensus group on congenital heart disease. *J Cardiovasc Magn Reson* 2013; **15**: 51. doi: http://dx.doi.org/10.1186/1532-429X-15-51
35. Devos DG, Kilner PJ. Calculations of cardiovascular shunts and regurgitation using magnetic resonance ventricular volume and aortic and pulmonary flow measurements. *Eur Radiol* 2010; **20**: 410–21. doi: http://dx.doi.org/10.1007/s00330-009-1568-2
36. Lankhaar JW, Hofman MB, Marcus JT, Zwanenburg JJ, Faes TJ, Vonk-Noordegraaf A. Correction of phase offset errors in main pulmonary artery flow quantification. *J Magn Reson Imaging* 2005; **22**: 73–9. doi: http://dx.doi.org/10.1002/jmri.20361
37. Holland BJ, Printz BF, Lai WW. Baseline correction of phase-contrast images in congenital cardiovascular magnetic resonance. *J Cardiovasc Magn Reson* 2010; **12**: 11. doi: http://dx.doi.org/10.1186/1532-429X-12-11
38. Sakuma H, Kawada N, Kubo H, Nishide Y, Takano K, Kato N, et al. Effect of breath holding on blood flow measurement using fast velocity encoded cine MRI. *Magn Reson Med* 2001; **45**: 346–8. doi: http://dx.doi.org/10.1002/1522-2594(200102)45:2<346::AID-MRM1044>3.0.CO;2-I
39. Ley S, Fink C, Puderbach M, Zaporozhan J, Plathow C, Eichinger M, et al. MRI Measurement of the hemodynamics of the pulmonary and systemic arterial circulation: influence of breathing maneuvers. *AJR Am J Roentgenol* 2006; **187**: 439–44. doi: http://dx.doi.org/10.2214/AJR.04.1738
40. Johansson B, Babu-Narayan SV, Kilner PJ. The effects of breath-holding on pulmonary regurgitation measured by cardiovascular magnetic resonance velocity mapping. *J Cardiovasc Magn Reson* 2009; **11**: 1. doi: http://dx.doi.org/10.1186/1532-429X-11-1
41. Abolmaali N, Seitz U, Esmaeili A, Kock M, Radeloff D, Ackermann H, et al. Evaluation of a resistance-based model for the quantification of pulmonary arterial hypertension using MR flow measurements. *J Magn Reson Imaging* 2007; **26**: 646–53. doi: http://dx.doi.org/10.1002/jmri.21059
42. Roldán-Alzate A, Frydrychowicz A, Johnson KM, Kellihan H, Chesler NC, Wieben O, et al. Non-invasive assessment of cardiac function and pulmonary vascular resistance in an canine model of acute thromboembolic pulmonary hypertension using 4D flow cardiovascular magnetic resonance. *J Cardiovasc Magn Reson* 2014; **16**: 23. doi: http://dx.doi.org/10.1186/1532-429X-16-23
43. Garcia-Álvarez A, Fernández-Friera L, García-Ruiz JM, Nuño-Ayala M, Pereda D, Fernández-Jimenez R, et al. Noninvasive monitoring of serial changes in pulmonary vascular resistance and acute vasodilator testing using cardiac magnetic resonance. *J Am Coll Cardiol* 2013; **62**: 1621–31. doi: http://dx.doi.org/10.1016/j.jacc.2013.07.037
44. Kang KW, Chang HJ, Kim YJ, Choi BW, Lee HS, Yang WI, et al. Cardiac magnetic resonance imaging-derived pulmonary artery distensibility index correlates with pulmonary artery stiffness and predicts

functional capacity in patients with pulmonary arterial hypertension. *Circ J* 2011; **75**: 2244–51. doi: http://dx.doi.org/10.1253/circj.CJ-10-1310

45. Stevens GR, Garcia-Alvarez A, Sahni S, Garcia MJ, Fuster V, Sanz J. RV dysfunction in pulmonary hypertension is independently related to pulmonary artery stiffness. *JACC Cardiovasc Imaging* 2012; **5**: 378–87. doi: http://dx.doi.org/10.1016/j.jcmg.2011.11.020
46. Swift AJ, Rajaram S, Condliffe R, Capener D, Hurdman J, Elliot C, et al. Pulmonary artery relative area change detects mild elevations in pulmonary vascular resistance and predicts adverse outcome in pulmonary hypertension. *Invest Radiol* 2012; **47**: 571–7. doi: http://dx.doi.org/10.1097/RLI.0b013e31826c4341
47. Sanz J, Kariisa M, Dellegrottaglie S, Prat-González S, Garcia MJ, Fuster V, et al. Evaluation of pulmonary artery stiffness in pulmonary hypertension with cardiac magnetic resonance. *JACC Cardiovasc Imaging* 2009; **2**: 286–95. doi: http://dx.doi.org/10.1016/j.jcmg.2008.08.007
48. Sanz J, Kuschnir P, Rius T, Salguero R, Sulica R, Einstein AJ, et al. Pulmonary arterial hypertension: noninvasive detection with phase-contrast MR imaging. *Radiology* 2007; **243**: 70–9. doi: http://dx.doi.org/10.1148/radiol.2431060477
49. Moral S, Fernández-Friera L, Stevens G, Guzman G, García-Alvarez A, Nair A, et al. New index alpha improves detection of pulmonary hypertension in comparison with other cardiac magnetic resonance indices. *Int J Cardiol* 2012; **161**: 25–30. doi: http://dx.doi.org/10.1016/j.ijcard.2011.04.024
50. García-Alvarez A, Fernández-Friera L, Mirelis JG, Sawit S, Nair A, Kallman J, et al. Non-invasive estimation of pulmonary vascular resistance with cardiac magnetic resonance. *Eur Heart J* 2011; **32**: 2438–45. doi: http://dx.doi.org/10.1093/eurheartj/ehr173
51. Helderman F, Mauritz GJ, Andringa KE, Vonk-Noordegraaf A, Marcus JT. Early onset of retrograde flow in the main pulmonary artery is a characteristic of pulmonary arterial hypertension. *J Magn Reson Imaging* 2011; **33**: 1362–8. doi: http://dx.doi.org/10.1002/jmri.22581
52. Truong U, Fonseca B, Dunning J, Burgett S, Lanning C, Ivy DD, et al. Wall shear stress measured by phase contrast cardiovascular magnetic resonance in children and adolescents with pulmonary arterial hypertension. *J Cardiovasc Magn Reson* 2013; **15**: 81. doi: http://dx.doi.org/10.1186/1532-429X-15-81
53. Rolf A, Rixe J, Kim WK, Guth S, Körlings N, Möllmann H, et al. Pulmonary vascular remodeling before and after pulmonary endarterectomy in patients with chronic thromboembolic pulmonary hypertension: a cardiac magnetic resonance study. *Int J Cardiovasc Imaging* 2015; **31**: 613–9. doi: http://dx.doi.org/10.1007/s10554-014-0580-z
54. Ley S, Kramm T, Kauczor HU, Mayer E, Heussel CP, Thelen M, et al. Pre- and postoperative assessment of hemodynamics in patients with chronic thromboembolic pulmonary hypertension by MR techniques. [In German.] *Rofo* 2003; **175**: 1647–54. doi: http://dx.doi.org/10.1055/s-2003-45340
55. Guo X, Liu M, Ma Z, Wang S, Yang Y, Zhai Z, et al. Flow characteristics of the proximal pulmonary arteries and vena cava in patients with chronic thromboembolic pulmonary hypertension: correlation between 3.0 T phase-contrast MRI and right heart catheterization. *Diagn Interv Radiol* 2014; **20**: 414–20. doi: http://dx.doi.org/10.5152/dir.2014.13501
56. Barker AJ, Roldán-Alzate A, Entezari P, Shah SJ, Chesler NC, Wieben O, et al. Four-dimensional flow assessment of pulmonary artery flow and wall shear stress in adult pulmonary arterial hypertension: results from two institutions. *Magn Reson Med* 2015; **73**: 1904–13. doi: http://dx.doi.org/10.1002/mrm.25326
57. Ley S, Fink C, Risse F, Ehlken N, Fischer C, Ley-Zaporozhan J, et al. Magnetic resonance imaging to assess the effect of exercise training on pulmonary perfusion and blood flow in patients with pulmonary hypertension. *Eur Radiol* 2013; **23**: 324–31. doi: http://dx.doi.org/10.1007/s00330-012-2606-z
58. Castelain V, Hervé P, Lecarpentier Y, Duroux P, Simonneau G, Chemla D. Pulmonary artery pulse pressure and wave reflection in chronic pulmonary thromboembolism and primary pulmonary hypertension. *J Am Coll Cardiol* 2001; **37**: 1085–92. doi: http://dx.doi.org/10.1016/S0735-1097(00)01212-2
59. Hardziyenka M, Reesink HJ, Bouma BJ, de Bruin-Bon HA, Campian ME, Tanck MW, et al. A novel echocardiographic predictor of in-hospital mortality and mid-term haemodynamic improvement after pulmonary endarterectomy for chronic thrombo-embolic pulmonary hypertension. *Eur Heart J* 2007; **28**: 842–9. doi: http://dx.doi.org/10.1093/eurheartj/ehl534
60. Klok FA, Romeih S, Westenberg JJ, Kroft LJ, Huisman MV, de Roos A. Pulmonary flow profile and distensibility following acute pulmonary embolism. *J Cardiovasc Magn Reson* 2011; **13**: 14. doi: http://dx.doi.org/10.1186/1532-429X-13-14
61. Kondo C, Caputo GR, Masui T, Foster E, O'Sullivan M, Stulbarg MS, et al. Pulmonary hypertension: pulmonary flow quantification and flow profile analysis with velocity-encoded cine MR imaging. *Radiology* 1992; **183**: 751–8. doi: http://dx.doi.org/10.1148/radiology.183.3.1584932
62. Mousseaux E, Tasu JP, Jolivet O, Simonneau G, Bittoun J, Gaux JC. Pulmonary arterial resistance: noninvasive measurement with indexes of pulmonary flow estimated at velocity-encoded MR imaging–preliminary experience. *Radiology* 1999; **212**: 896–902. doi: http://dx.doi.org/10.1148/radiology.212.3.r99au21896
63. Quail MA, Knight DS, Steeden JA, Taelman L, Moledina S, Taylor AM, et al. Non-invasive pulmonary artery wave intensity analysis in pulmonary hypertension. *Am J Physiol Heart Circ Physiol* 2015; **308**: H1603–11. doi: http://dx.doi.org/10.1152/ajpheart.00480.2014
64. Sugimoto M, Kajino H, Kajihama A, Nakau K, Murakami N, Azuma H. Assessment of pulmonary arterial pressure by velocity-encoded cine magnetic resonance imaging in children with congenital heart disease. *Circ J* 2013; **77**: 3015–22. doi: http://dx.doi.org/10.1253/circj.CJ-13-0626
65. Muthurangu V, Taylor A, Andriantsimiavona R, Hegde S, Miquel ME, Tulloh R, et al. Novel method of quantifying pulmonary vascular resistance by use of simultaneous invasive pressure monitoring and phase-contrast magnetic resonance flow. *Circulation* 2004; **110**: 826–34. doi: http://dx.doi.org/10.1161/01.CIR.0000138741.72946.84
66. Kreitner KF, Wirth GM, Krummenauer F, Weber S, Pitton MB, Schneider J, et al. Noninvasive assessment of pulmonary hemodynamics in patients with chronic thromboembolic pulmonary hypertension by high temporal resolution phase-contrast MRI: correlation with simultaneous invasive pressure recordings. *Circ Cardiovasc Imaging* 2013; **6**: 722–9. doi: http://dx.doi.org/10.1161/CIRCIMAGING.112.000276
67. Mauritz GJ, Marcus JT, Boonstra A, Postmus PE, Westerhof N, Vonk-Noordegraaf A. Non-invasive stroke volume assessment in patients with pulmonary arterial hypertension: left-sided data mandatory. *J Cardiovasc Magn Reson* 2008; **10**: 51. doi: http://dx.doi.org/10.1186/1532-429X-10-51

68. O'Brien KR, Cowan BR, Jain M, Stewart RA, Kerr AJ, Young AA. MRI phase contrast velocity and flow errors in turbulent stenotic jets. *J Magn Reson Imaging* 2008; **28**: 210–8. doi: http://dx.doi.org/10.1002/jmri.21395
69. Nordmeyer S, Riesenkampff E, Messroghli D, Kropf S, Nordmeyer J, Berger F, et al. Four-dimensional velocity-encoded magnetic resonance imaging improves blood flow quantification in patients with complex accelerated flow. *J Magn Reson Imaging* 2013; **37**: 208–16. doi: http://dx.doi.org/10.1002/jmri.23793
70. Hoeper MM. Definition, classification, and epidemiology of pulmonary arterial hypertension. *Semin Respir Crit Care Med* 2009; **30**: 369–75. doi: http://dx.doi.org/10.1055/s-0029-1233306
71. Chernobelsky A, Shubayev O, Comeau CR, Wolff SD. Baseline correction of phase contrast images improves quantification of blood flow in the great vessels. *J Cardiovasc Magn Reson* 2007; **9**: 681–5. doi: http://dx.doi.org/10.1080/10976640601187588
72. Rigsby CK, Hilpipre N, McNeal GR, Zhang G, Boylan EE, Popescu AR, et al. Analysis of an automated background correction method for cardiovascular MR phase contrast imaging in children and young adults. *Pediatr Radiol* 2014; **44**: 265–73. doi: http://dx.doi.org/10.1007/s00247-013-2830-y
73. Bane O, Shah SJ, Cuttica MJ, Collins JD, Selvaraj S, Chatterjee NR, et al. A non-invasive assessment of cardiopulmonary hemodynamics with MRI in pulmonary hypertension. *Magn Reson Imaging* 2015; **33**: 1224–35. doi: http://dx.doi.org/10.1016/j.mri.2015.08.005
74. Laffon E, Vallet C, Bernard V, Montaudon M, Ducassou D, Laurent F, et al. A computed method for noninvasive MRI assessment of pulmonary arterial hypertension. *J Appl Physiol (1985)* 2004; **96**: 463–8.
75. Rich S, D'Alonzo GE, Dantzker DR, Levy PS. Magnitude and implications of spontaneous hemodynamic variability in primary pulmonary hypertension. *Am J Cardiol* 1985; **55**: 159–63. doi: http://dx.doi.org/10.1016/0002-9149(85)90319-4
76. Reiter G, Reiter U, Kovacs G, Kainz B, Schmidt K, Maier R, et al. Magnetic resonance-derived 3-dimensional blood flow patterns in the main pulmonary artery as a marker of pulmonary hypertension and a measure of elevated mean pulmonary arterial pressure. *Circ Cardiovasc Imaging* 2008; **1**: 23–30. doi: http://dx.doi.org/10.1161/CIRCIMAGING.108.780247
77. Odagiri K, Inui N, Miyakawa S, Hakamata A, Wei J, Takehara Y, et al. Abnormal hemodynamics in the pulmonary artery seen on time-resolved 3-dimensional phase-contrast magnetic resonance imaging (4D-flow) in a young patient with idiopathic pulmonary arterial hypertension. *Circ J* 2014; **78**: 1770–2. doi: http://dx.doi.org/10.1253/circj.CJ-14-0283
78. Ota H, Sugimura K, Miura M, Shimokawa H. Four-dimensional flow magnetic resonance imaging visualizes drastic change in vortex flow in the main pulmonary artery after percutaneous transluminal pulmonary angioplasty in a patient with chronic thromboembolic pulmonary hypertension. *Eur Heart J* 2015; **36**: 1630. doi: http://dx.doi.org/10.1093/eurheartj/ehv054
79. Reiter G, Reiter U, Kovacs G, Olschewski H, Fuchsjäger M. Blood flow vortices along the main pulmonary artery measured with MR imaging for diagnosis of pulmonary hypertension. *Radiology* 2015; **275**: 71–9. doi: http://dx.doi.org/10.1148/radiol.14140849
80. Reiter U, Reiter G, Kovacs G, Stalder AF, Gulsun MA, Greiser A, et al. Evaluation of elevated mean pulmonary arterial pressure based on magnetic resonance 4D velocity mapping: comparison of visualization techniques. *PLoS One* 2013; **8**: e82212. doi: http://dx.doi.org/10.1371/journal.pone.0082212
81. Bächler P, Pinochet N, Sotelo J, Crelier G, Irarrazaval P, Tejos C, et al. Assessment of normal flow patterns in the pulmonary circulation by using 4D magnetic resonance velocity mapping. *Magn Reson Imaging* 2013; **31**: 178–88. doi: http://dx.doi.org/10.1016/j.mri.2012.06.036
82. François CJ, Srinivasan S, Schiebler ML, Reeder SB, Niespodzany E, Landgraf BR, et al. 4D cardiovascular magnetic resonance velocity mapping of alterations of right heart flow patterns and main pulmonary artery hemodynamics in tetralogy of Fallot. *J Cardiovasc Magn Reson* 2012; **14**: 16. doi: http://dx.doi.org/10.1186/1532-429X-14-16
83. Lankhaar JW, Westerhof N, Faes TJ, Gan CT, Marques KM, Boonstra A, et al. Pulmonary vascular resistance and compliance stay inversely related during treatment of pulmonary hypertension. *Eur Heart J* 2008; **29**: 1688–95. doi: http://dx.doi.org/10.1093/eurheartj/ehn103
84. Bradlow WM, Gatehouse PD, Hughes RL, O'Brien AB, Gibbs JS, Firmin DN, et al. Assessing normal pulse wave velocity in the proximal pulmonary arteries using transit time: a feasibility, repeatability, and observer reproducibility study by cardiovascular magnetic resonance. *J Magn Reson Imaging* 2007; **25**: 974–81. doi: http://dx.doi.org/10.1002/jmri.20888
85. Peng HH, Chung HW, Yu HY, Tseng WY. Estimation of pulse wave velocity in main pulmonary artery with phase contrast MRI: preliminary investigation. *J Magn Reson Imaging* 2006; **24**: 1303–10. doi: http://dx.doi.org/10.1002/jmri.20782
86. Ibrahim el-SH, Shaffer JM, White RD. Assessment of pulmonary artery stiffness using velocity-encoding magnetic resonance imaging: evaluation of techniques. *Magn Reson Imaging* 2011; **29**: 966–74. doi: http://dx.doi.org/10.1016/j.mri.2011.04.012
87. Tang BT, Pickard SS, Chan FP, Tsao PS, Taylor CA, Feinstein JA. Wall shear stress is decreased in the pulmonary arteries of patients with pulmonary arterial hypertension: an image-based, computational fluid dynamics study. *Pulm Circ* 2012; **2**: 470–6. doi: http://dx.doi.org/10.4103/2045-8932.105035
88. Katritsis D, Kaiktsis L, Chaniotis A, Pantos J, Efstathopoulos EP, Marmarelis V. Wall shear stress: theoretical considerations and methods of measurement. *Prog Cardiovasc Dis* 2007; **49**: 307–29. doi: http://dx.doi.org/10.1016/j.pcad.2006.11.001
89. Barker AJ, Lanning C, Shandas R. Quantification of hemodynamic wall shear stress in patients with bicuspid aortic valve using phase-contrast MRI. *Ann Biomed Eng* 2010; **38**: 788–800. doi: http://dx.doi.org/10.1007/s10439-009-9854-3
90. Stalder AF, Russe MF, Frydrychowicz A, Bock J, Hennig J, Markl M. Quantitative 2D and 3D phase contrast MRI: optimized analysis of blood flow and vessel wall parameters. *Magn Reson Med* 2008; **60**: 1218–31. doi: http://dx.doi.org/10.1002/mrm.21778
91. Tuder RM. Pathology of pulmonary arterial hypertension. *Semin Respir Crit Care Med* 2009; **30**: 376–85. doi: http://dx.doi.org/10.1055/s-0029-1233307
92. Mutlak D, Aronson D, Lessick J, Reisner SA, Dabbah S, Agmon Y. Functional tricuspid regurgitation in patients with pulmonary hypertension: is pulmonary artery pressure the only determinant of regurgitation severity? *Chest* 2009; **135**: 115–21. doi: http://dx.doi.org/10.1378/chest.08-0277
93. Westenberg JJ, Roes SD, Ajmone Marsan N, Binnendijk NM, Doornbos J, Bax JJ, et al. Mitral valve and tricuspid valve blood flow: accurate quantification with 3D velocity-encoded MR imaging with retrospective valve tracking. *Radiology* 2008; **249**:

792–800. doi: http://dx.doi.org/10.1148/radiol.2492080146

94. Roes SD, Hammer S, van der Geest RJ, Marsan NA, Bax JJ, Lamb HJ, et al. Flow assessment through four heart valves simultaneously using 3-dimensional 3-directional velocity-encoded magnetic resonance imaging with retrospective valve tracking in healthy volunteers and patients with valvular regurgitation. *Invest Radiol* 2009; **44**: 669–75. doi: http://dx.doi.org/10.1097/RLI.0b013e3181ae99b5
95. Hsiao A, Tariq U, Alley MT, Lustig M, Vasanawala SS. Inlet and outlet valve flow and regurgitant volume may be directly and reliably quantified with accelerated, volumetric phase-contrast MRI. *J Magn Reson Imaging* 2015; **41**: 376–85. doi: http://dx.doi.org/10.1002/jmri.24578
96. Nogami M, Ohno Y, Koyama H, Kono A, Takenaka D, Kataoka T, et al. Utility of phase contrast MR imaging for assessment of pulmonary flow and pressure estimation in patients with pulmonary hypertension: comparison with right heart catheterization and echocardiography. *J Magn Reson Imaging* 2009; **30**: 973–80. doi: http://dx.doi.org/10.1002/jmri.21935
97. Carlsson M, Heiberg E, Toger J, Arheden H. Quantification of left and right ventricular kinetic energy using four-dimensional intracardiac magnetic resonance imaging flow measurements. *Am J Physiol Heart Circ Physiol* 2012; **302**: H893–900. doi: http://dx.doi.org/10.1152/ajpheart.00942.2011
98. Fredriksson AG, Svalbring E, Eriksson J, Dyverfeldt P, Alehagen U, Engvall J, et al. 4D flow MRI can detect subtle right ventricular dysfunction in primary left ventricular disease. *J Magn Reson Imaging* 2016; **43**: 558–65. doi: http://dx.doi.org/10.1002/jmri.25015
99. Han QJ, Witschey WR, Fang-Yen CM, Arkles JS, Barker AJ, Forfia PR, et al. Altered right ventricular kinetic energy work density and viscous energy dissipation in patients with Pulmonary Arterial Hypertension: a pilot study using 4D flow MRI. *PLoS One* 2015; **10**: e0138365. doi: http://dx.doi.org/10.1371/journal.pone.0138365
100. Fenster BE, Browning J, Schroeder JD, Schafer M, Podgorski CA, Smyser J, et al. Vorticity is a marker of right ventricular diastolic dysfunction. *Am J Physiol Heart Circ Physiol* 2015; **309**: H1087–93. doi: http://dx.doi.org/10.1152/ajpheart.00278.2015
101. Ibrahim el-SH, White RD. Cardiovascular magnetic resonance for the assessment of pulmonary arterial hypertension: toward a comprehensive CMR exam. *Magn Reson Imaging* 2012; **30**: 1047–58. doi: http://dx.doi.org/10.1016/j.mri.2012.03.001
102. Vonk-Noordegraaf A, Souza R. Cardiac magnetic resonance imaging: what can it add to our knowledge of the right ventricle in pulmonary arterial hypertension? *Am J Cardiol* 2012; **110**: 25S–31S. doi: http://dx.doi.org/10.1016/j.amjcard.2012.06.013
103. Bollache E, Redheuil A, Clement-Guinaudeau S, Defrance C, Perdrix L, Ladouceur M, et al. Automated left ventricular diastolic function evaluation from phase-contrast cardiovascular magnetic resonance and comparison with Doppler echocardiography. *J Cardiovasc Magn Reson* 2010; **12**: 63. doi: http://dx.doi.org/10.1186/1532-429X-12-63